Sedimentology (2003) **50,** 703–724 doi: 10.1046/j.1365-3091.2003.00571.x

Petrography and chemistry of sandstones from the Swiss Molasse Basin: an archive of the Oligocene to Miocene evolution of the Central Alps

HILMAR VON EYNATTEN
Geowissenschaftliches Zentrum der Universität Göttingen, Abteilung Sedimentologie/Umweltgeologie, Goldschmidtstrasse 3, D-37077 Göttingen, Germany (E-mail: hilmar.von.eynatten@geo.uni-goettingen.de)

ABSTRACT

Oligocene to Miocene fluvial sandstones from the Swiss Molasse Basin were analysed for sandstone framework composition, heavy minerals, whole-rock geochemistry and detrital chrome spinel chemistry. Samples were taken from the proximal part of the basin close to the Alpine main thrust and are chronostratigraphically calibrated between 31 and 13 Ma. Sandstone composition allows the identification of different source rocks, and their variation in time and space place constraints on the Oligocene to Miocene evolution of the Central Alps. In the eastern part of the basin, sandstones document a normal unroofing sequence with the downcutting from Austroalpine sedimentary cover into Austroalpine crystalline rocks and, slightly later at $\approx$21 Ma, into Penninic ophiolites. In the central part, downcutting into crystalline basement rocks occurred at $\approx$25 Ma, and the removal of the sedimentary cover was much more advanced than in the east. This may be interpreted as a first signal from the doming of the Lepontine area. At $\approx$20 Ma, extensional tectonics in the hinterland led to the first exposure of low-grade metamorphic rocks from the footwall of the Simplon Fault in the Central Alps. Erosion of these rocks persisted up to the youngest sediments at $\approx$13 Ma. In the western part of the basin, a contribution from granitoid and (ultra)mafic rocks is documented as early as $\approx$28 Ma. The source for the (ultra)mafic detritus is Penninic ophiolites from the Piemonte zone of the western Alps, which were already exposed at the surface at that time.

Keywords Central Alps, geochemistry, heavy minerals, provenance, sandstone petrography, Swiss Molasse Basin.

INTRODUCTION

Sediment composition is controlled by a complex suite of parameters starting with the initial source rock composition and followed by the various processes that modify the sediment on its way from the source area to its present-day location in outcrops or in the subsurface (e.g. Johnsson, 1993). In coarse-grained first-cycle sediments with good provenance control, e.g. alluvial-fan sediments deposited close to the thrust front of mountain ranges, the influence of modifying processes is greatly decreased because of the short time span between first exposure in the source area and final deposition. In such cases, changes in sediment composition may then be directly related to the tectonic evolution of the hinterland (e.g. Colombo, 1994).

The Swiss Molasse Basin and the adjacent Central Alps of Switzerland provide a natural laboratory to study the response of sediment composition to late orogenic processes because (1) the source area of most of the Swiss Molasse deposits, i.e. the Central Alps, is still exposed and among the best known orogens worldwide (e.g. Schmid *et al.*, 1996); and (2) the sediments of the Swiss Molasse Basin have been examined in detail with respect to facies and basin analysis as well as heavy mineral distribution and are precisely dated by mammal biostratigraphy and

magnetostratigraphy (see Geological Setting). The latter is almost unique because fossils are generally rare in coarse-grained fluvial deposits, and thus the biostratigraphic calibration of such sediments is usually poor (e.g. Tertiary Himalayan foreland basin; Najman & Garzanti, 2000).

Systematic studies of the sedimentology and composition of sandstones from the Swiss Molasse Basin started in the 1950s and 1960s, and focused on grain-size analysis, conglomerate composition and heavy minerals, as well as feldspar and carbonate content (Matter, 1964; Füchtbauer, 1964, 1967 and references therein). More recently, extensive studies on facies, heavy minerals and seismic lines were carried out in combination with mammal biostratigraphy and magnetostratigraphy throughout the basin (Allen *et al.*, 1985; Pfiffner, 1986; Burbank *et al.*, 1992; Schlunegger *et al.*, 1996, 1997; Kempf *et al.*, 1997, 1999; Strunck, 2001) leading to a detailed picture of basin evolution and its relation to Alpine orogenic processes (Sinclair & Allen, 1992; Burkhard & Sommaruga, 1998; Schlunegger *et al.*, 1998; Schlunegger, 1999; Kuhlemann & Kempf, 2002). Geochronological studies of detrital minerals provide additional information on the thermal history of the hinterland (von Eynatten *et al.*, 1999; Spiegel *et al.*, 2000; von Eynatten & Wijbrans, 2003).

The aim of this study is (1) to provide a comprehensive view of the compositional evolution of proximal sandstones from the Swiss Molasse Basin in space and time; and (2) to discuss the implications of the compositional evolution of the sandstones for the Oligocene to Miocene evolution of the Central Alps. In addition, different analytical approaches to sandstone composition are compared to evaluate the strength of each method for unravelling specific source characteristics.

GEOLOGICAL SETTING

The Swiss Molasse Basin (SMB; Fig. 1) refers to the western part of the North Alpine Foreland Basin, which formed on European lithosphere by flexural bending in response to the tectonic load imposed by the northward-propagating Alpine orogen (Homewood *et al.*, 1986). The SMB strikes from Savoy (France) in the west to Lake Constance in the east and forms a classical peripheral foredeep along the northern side of the central Alps. In cross-sections, the basin exhibits a strong asymmetric shape with its deepest parts (> 4 km below sea level) lying directly adjacent to the Alpine thrust front. The southern rim of exposed strata of the SMB is present in a stack of S-dipping thrust sheets (see Subalpine Molasse; Fig. 1). Molasse deposits further to the north of the Subalpine Molasse are essentially undeformed (Plateau Molasse), although later incorporated into the Alpine thrust belt and transported piggy-back-like towards the northwest. Subsequent uplift and erosion of the entire SMB started at about Late Serravallian time 12–11 Ma; (Berger, 1996; Kuhlemann & Kempf, 2002).

The sedimentary record of the Oligocene to Miocene SMB is characterized by two regressive megacycles each starting with marine deposits that grade upsection into clastic fluvial deposits. The first cycle started in the Rupelian with the Lower Marine Molasse (UMM) and lasted up to the Aquitanian (Lower Freshwater Molasse; USM); the second cycle started with the Burdigalian transgression (Upper Marine Molasse; OMM) and ended with Serravalian fluvial clastics of the Upper Freshwater Molasse (OSM; Berger, 1996). During the fluvial stages, the basin was dominated by wide meander belts with axial drainage to the NE (first cycle) and later to the SW (second cycle). Both marine and fluvial deposits interfinger with transverse alluvial fan systems. The latter delivered coarse-grained detritus from the prograding orogenic wedge of the Central Alps (Schlunegger *et al.*, 1997; Kuhlemann & Kempf, 2002).

The Central Alps, which form the hinterland for the sediments of the SMB, constitute a doubly vergent orogen with high-grade metamorphic rocks of the Lepontine dome in its core (Schmid *et al.*, 1996; Fig. 1). The southern flank, comprising the unmetamorphosed south-vergent South Alpine basement and sedimentary cover nappes, is separated from the Lepontine dome by the Insubric Line. The southern Alps are not relevant to this study in terms of potential source areas, because the drainage divide was located north of the Insubric line throughout Oligocene to Miocene times (Schlunegger *et al.*, 1998). The northern flank comprises the north-vergent stack of low- to medium-grade metamorphic to unmetamorphosed Helvetic, Penninic and Austroalpine basement and cover nappes (Fig. 1). The Helvetic nappes comprise mostly carbonate rocks. The external (Helvetic) basement massifs were not yet exhumed at the time of Molasse sedimentation (Michalski & Soom, 1990). Penninic units are mostly composed of Cretaceous flysch, granitoids, ophiolites and high-grade metamorphic rocks exposed in the

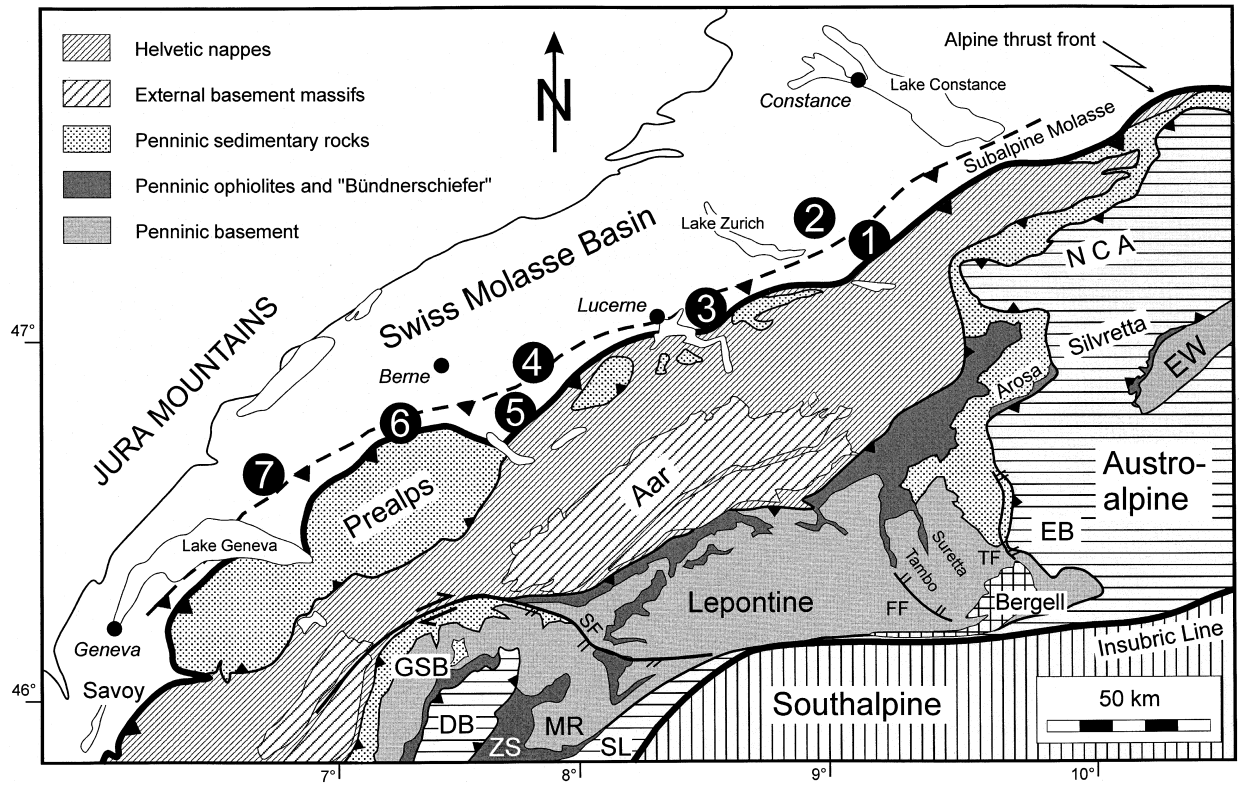

Fig. 1. Sketch map of the Central Alps showing major structural units and the Swiss Molasse Basin (SMB) north of the main Alpine thrust. Stippled thrust indicates transition between Subalpine Molasse and Plateau Molasse. Numbers 1–7 indicate location of the investigated composite sections. DB, Dent Blanche; EB, Err-Bernina; EW, Engadine window; FF, Forcola Fault; GSB, Grand St Bernard; MR, Monte Rosa; NCA, Northern Calcareous Alps; SF, Simplon Fault zone; SL, Sesia–Lanzo; TF, Turba Fault zone; ZS, Zermatt-Saas zone. Modified after Frey & Ferreiro Mählmann (1999).

Lepontine dome (Fig. 1). The Austroalpine units comprise mostly carbonate rocks in the Northern Calcareous Alps (NCA) and crystalline basement rocks further to the south (Silvretta, Err-Bernina) and in the west (Dent-Blanche).

The peak of Alpine greenschist to amphibolite facies metamorphism in the western and central Alps is dated at 36–40 Ma (Steck & Hunziker, 1994; Desmons *et al.*, 1999) and 32–33 Ma (Gebauer, 1999) respectively. Emplacement of the Penninic and Austroalpine nappes occurred before 35 Ma (Schmid *et al.*, 1996; Markley *et al.*, 1998). Detachment of the Prealps, which form part of the former sedimentary cover of Penninic basement units, and their emplacement onto Helvetic units (Fig. 1) was also before the onset of Molasse sedimentation. Subsequent crustal shortening and northward progradation of the thrust front along the main Alpine thrust (Fig. 1) led to the accretion of Molasse strata to the orogenic wedge (Pfiffner, 1986; Kempf *et al.*, 1999).

The high-grade metamorphic rocks of the Lepontine dome are separated from the hanging-wall units to the west (Austroalpine-Piedmont nappe stack; Dal Piaz, 1999) by the Simplon Fault (SF; Fig. 1), a major detachment fault accommodating Late Oligocene to Recent lateral extension in the Central Alps. Exhumation of the Lepontine dome started at ≈30 Ma (e.g. Hurford *et al.*, 1989; Gebauer, 1999). Enhanced rates of displacement along the SF and exhumation of the Lepontine dome occurred at 18–15 Ma (Grasemann & Mancktelow, 1993). To the east, Penninic units of the Lepontine dome are separated from structurally higher upper Penninic nappes (Tambo, Suretta) by steeply inclined E-dipping normal faults (e.g. Forcola Fault, Fig. 1; Baudin *et al.*, 1993).

SAMPLED DRAINAGE SYSTEMS AND CHRONOSTRATIGRAPHIC CALIBRATION

In this study, sampling was restricted to chronostratigraphically well-constrained sections (Fig. 2)

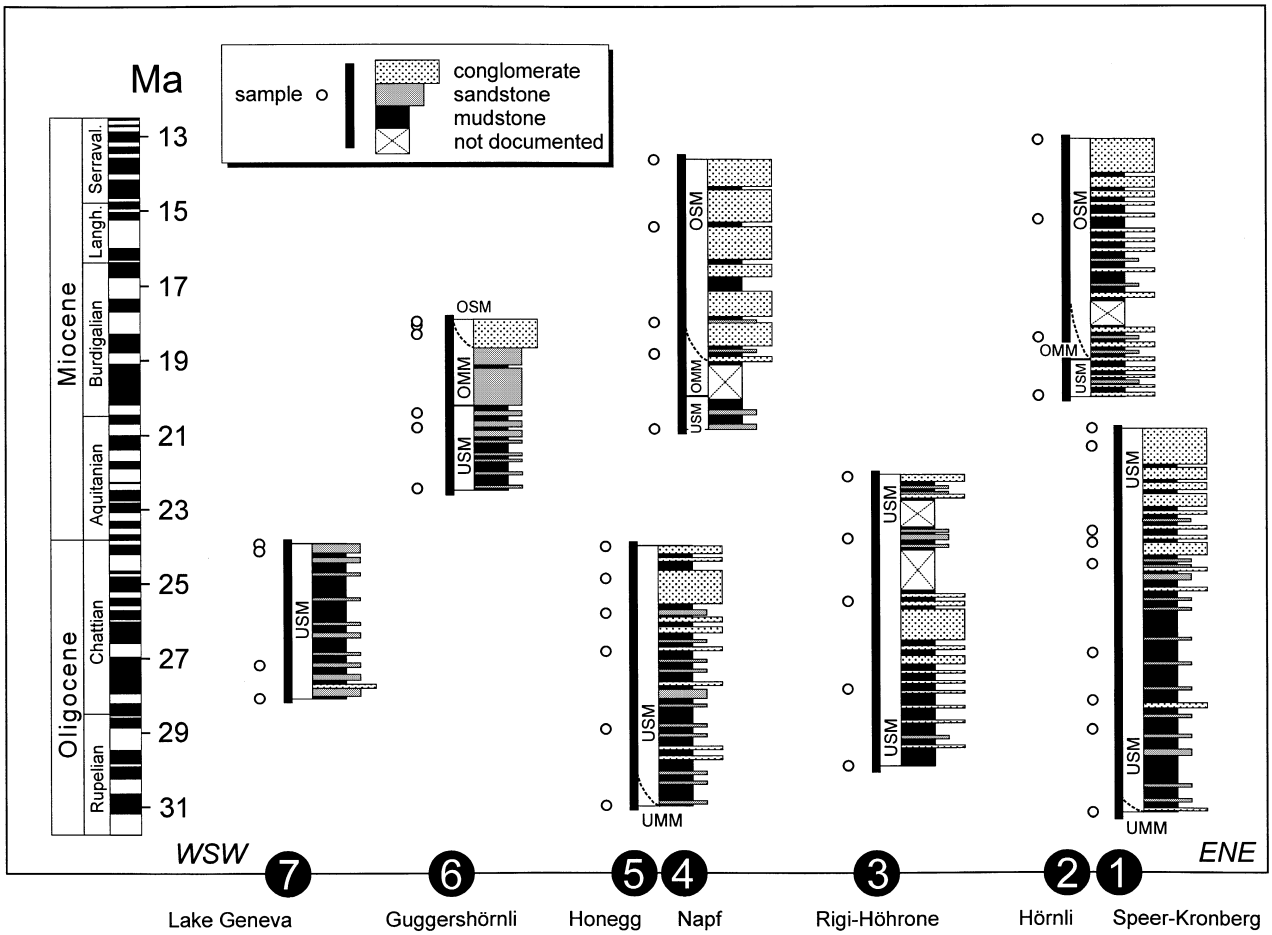

Fig. 2. Sampled sections (drainage systems) and their position in time and space within the SMB. Sedimentary and stratigraphic data are compiled from Kempf *et al.* (1999), Schlunegger *et al.* (1996, 1997) and Strunck (2001). Time scale after Berggren *et al.* (1995). Locations refer to Fig. 1. UMM, Lower Marine Molasse; USM, Lower Freshwater Molasse; OMM, Upper Marine Molasse; OSM, Upper Freshwater Molasse.

from transverse drainage systems to mimimize (1) uncertainties in the stratigraphic age of the analysed samples and (2) problems of mixing with sediment derived from axial drainage systems. In fact, the errors on 'absolute' sedimentation ages are mostly in the range of a few hundred thousand years (Table 1). The only axial drainage system that was sampled is the Lake Geneva dispersal system (Section 7): (1) because of its strong influence on the Chattian to Aquitanian axial drainage system of the SMB (Maurer, 1983); and (2) to obtain control on possible mixing of transverse and axial dispersal systems.

Analysed samples represent ≈ 2 Ma intervals and, as such, allow the compositional evolution of sandstones in each section to be evaluated in relatively small time slices. Where additional information suggests major changes in sediment composition, smaller time intervals were sampled. A total of 39 samples were collected from seven composite sections between Lake Geneva and Lake Constance (Table 1, Figs 1 and 2). Previous studies of these sections (Schlunegger, 1995; Kempf, 1998; Strunck, 2001) provide a dense network of heavy mineral data, which coincide well with the heavy mineral data obtained from the 39 samples in this study. Therefore, all samples are considered to be representative of the compositional evolution of the more proximal sediments of the SMB close to the Alpine thrust front. For details of the sedimentological evolution, the reader is referred to the aforementioned studies. The sampled sections represent the following palaeodrainage systems (Fig. 3).

(1) Speer/Kronberg alluvial fan system

This major dispersal system in the Rupelian to Aquitanian eastern SMB drained the present-day

Table 1. Sample description, localities, magnetostratigraphically calibrated ages with references and available data sets.

Sample	Lithology	Section	Locality (Fig. 1)	Age (Ma)	Reference	Available data sets*			
						hm	lm	chem	$^{40}Ar/^{39}Ar$
EY 18-1	Fine–medium litharenite	Fischenbach, Schwarzenberg	4	20·9 ± 0·1	Schlunegger *et al.* (1996)	+	+	+	+
EY 18-2	Medium litharenite	Rigi, Fischchrattenbach	3	29·8 ± 0·2	Schlunegger *et al.* (1996)	+	+	+	+
EY 18-3	Medium litharenite	Rigi, Fischchrattenbach–Seebodenalp	3	27·8 ± 0·2	Schlunegger *et al.* (1996)	+	+	+	–
EY 18-4	Medium–coarse litharenite	Rigi, Felsenweg	3	25·5 ± 1·0	Schlunegger *et al.* (1996)	+	+	+	–
EY 18-6	Medium litharenite	Höhrone, Nettenbach, Sihl-Tal	3	23·8 ± 0·1	Schlunegger *et al.* (1996)	+	+	+	–
EY 18-7	Medium litharenite	Höhrone, Nettenbach	3	22·1 ± 0·3	Schlunegger *et al.* (1996)	+	+	+	+
EY 18-8	Medium litharenite	Fontannen, Unter dem Hengst	4	13·6 ± 0·1	Schlunegger *et al.* (1996), Kempf *et al.* (1997)	+	+	+	+
EY 18-9	Medium–coarse litharenite	Marbach, Steiglenbach	5	28·9 ± 0·2	Schlunegger *et al.* (1996)	+	+	+	–
EY 18-10	Fine–medium litharenite	Honegg, Schwarzbach	5	26·8 ± 0·2	Schlunegger *et al.* (1996)	+	+	+	–
EY 18-11	Fine–medium litharenite	Schwändigraben, Eschholzmatt	4	18·9 ± 0·2	Schlunegger *et al.* (1996), Kempf *et al.* (1997)	+	+	+	+
EY 18-12	Medium litharenite	Schwändigraben, Alp Wittenschwändi	4	18·0 ± 0·3	Schlunegger *et al.* (1996), Kempf *et al.* (1997)	+	+	+	+
EY 18-13	Medium litharenite	Fontannen, Seeblibach	4	15·4 ± 0·6	Schlunegger *et al.* (1996), Kempf *et al.* (1997)	+	+	+	+
EY 18-14	Medium litharenite	Waldemme, Schüpfheim	5	31·0 ± 0·2	Schlunegger *et al.* (1996)	+	+	+	+
EY 18-15	Medium litharenite	Prässerebach, Teuffenthal	5	25·8 ± 0·1	Schlunegger *et al.* (1996)	+	+	+	–
EY 18-16	Fine litharenite	Prässerebach, Dürrenschwendbach	5	24·9 ± 0·2	Schlunegger *et al.* (1996)	+	+	+	+
EY 18-17	Medium–coarse litharenite	Grunten, Thuner See	5	24·0 ± 0·2	Schlunegger *et al.* (1993, 1996)	+	+	+	–
EY 19-1	Medium litharenite	Thur section, Neslau	1	31·1 ± 0·2	Kempf *et al.* (1997, 1999)	+	+	+	–
EY 19-2	Medium litharenite	Thur section, Neslau	1	28·9 ± 0·2	Kempf *et al.* (1997, 1999)	+	+	+	+
EY 19-3	Fine litharenite	Necker section	1	21·2 ± 0·2	Kempf *et al.* (1997, 1999)	+	+	+	+
EY 19-4	Fine–medium litharenite	Necker section	1	23·9 ± 0·1	Kempf *et al.* (1997, 1999)	+	+	+	+
EY 19-5	Fine–medium litharenite	Necker section	1	23·6 ± 0·1	Kempf *et al.* (1997, 1999)	+	+	+	–
EY 19-6	Fine litharenite	Necker section	1	24·5 ± 0·2	Kempf *et al.* (1997, 1999)	+	+	+	–
EY 19-7	Fine–medium litharenite	Necker section	1	20·9 ± 0·1	Kempf *et al.* (1997, 1999)	+	+	+	–
EY 19-9	Fine litharenite	Necker section	1	26·9 ± 0·2	Kempf *et al.* (1997, 1999)	+	+	+	–
EY 19-10	Medium litharenite	Necker section	1	28·1 ± 0·2	Kempf *et al.* (1997, 1999)	+	+	+	–
EY 19-11	Fine litharenite	Goldinger Tobel section, OE Neuhaus	2	20·0 ± 0·2	Kempf *et al.* (1997, 1999)	+	+	+	+
EY 19-12	Fine litharenite	Goldinger Tobel section, top	2	18·4 ± 0·2	Kempf *et al.* (1997, 1999)	+	+	+	–
EY 19-13	Fine–medium litharenite	Hörnli section, 980 NN	2	13·2 ± 0·2	Kempf *et al.* (1997, 1999)	+	+	+	+
EY 19-14	Fine–medium litharenite	Jona section, Neuhof	2	15·1 ± 0·1	Kempf *et al.* (1997, 1999)	+	+	+	+
EY 21-1	Medium litharenite	Heitenried section	6	20·4 ± 0·2	Strunck (2001)	+	+	+	+
EY 21-2	Medium litharenite	Sensegraben section	6	18·4 ± 0·2	Strunck (2001)	+	+	+	–
EY 21-3	Medium litharenite	Sensegraben section	6	18·1 ± 0·2	Strunck (2001)	+	+	+	–

Table 1. Continued

Sample	Lithology	Section	Locality (Fig. 1)	Age (Ma)	Reference	Available data sets*			
						hm	lm	chem	$^{40}Ar/^{39}Ar$
EY 21-4	Medium litharenite	Sensegraben section	6	17·9 ± 0·2	Strunck (2001)	+	+	+	+
EY 21-5	Fine–medium litharenite	Sachlisgraben section, base	6	22·5 ± 0·1	Strunck (2001)	+	+	+	+
EY 21-6	Medium litharenite	Dürrbachgraben section, top	6	20·8 ± 0·2	Strunck (2001)	+	+	+	–
EY 21-7	Fine–medium litharenite	Talent southern section	7	28·1 ± 0·2	Strunck (2001)	+	+	+	+
EY 21-8	Fine–medium litharenite	Talent southern section	7	27·2 ± 0·8	Strunck (2001)	+	+	+	+
EY 21-9	Very fine–fine litharenite	Talent southern section	7	24·0 ± 0·1	Strunck (2001)	+	–	+	–
EY 21-10	Fine–medium litharenite	Talent southern section	7	23·9 ± 0·1	Strunck (2001)	+	+	+	+

* hm, heavy minerals; lm, light minerals; chem, major and trace elements; for $^{40}Ar/^{39}Ar$ ages of detrital white mica, see von Eynatten *et al.* (1999) and von Eynatten & Wijbrans (2003).

boundary area between the central and eastern Alps (Kempf *et al.*, 1999). The apex of the older Speer alluvial fan was located about 15 km SE of the eastern end of Lake Zurich and later moved about 20 km in a north-easterly direction to form the apex of the younger Kronberg alluvial fan. Nine samples were taken representing chronostratigraphic levels between 31·1 Ma and 20·9 Ma (Kempf, 1998).

(2) Hörnli alluvial fan system

In the Early Burdigalian, a new alluvial fan system developed that constitutes the major dispersal system in the eastern SMB up to the Middle Serravallian (Kempf *et al.*, 1999). The apex of the Hörnli alluvial fan was initially located about 15 km NE of the eastern end of Lake Zurich but subsequently propagated north-(west)ward during the Langhian to Serravallian. Four samples were taken representing chronostratigraphic levels between 20·0 Ma and 13·2 Ma (Kempf *et al.*, 1997).

(3) Rigi/Höhrone alluvial fan system

The Rigi alluvial fan was active from Late Rupelian to Early Chattian time (≈ 30 Ma to ≈ 25·5 Ma) in an area directly east of Lake Lucerne (Schlunegger *et al.*, 1997). The succession reflects a coarsening-upward megasequence from alluvial plain sediments including conglomeratic channel fills to massive conglomerates of an alluvial fan. A second coarsening-upward megasequence developed about 10 km to the NE in latest Chattian to Aquitanian time (≈ 24 to ≈ 22 Ma, Höhrone alluvial fan). Five samples were taken representing chronostratigraphic levels between 29·8 Ma and 22·1 Ma (Schlunegger *et al.*, 1997).

(4) Napf alluvial fan system

At the time of the Burdigalian marine ingression (OMM), the Napf alluvial megafan was established in the central SMB ≈ 30 km east of Berne. It is composed of continuously northward-prograding conglomeratic deposits documenting the time span from ≈ 20 Ma to ≈ 13 Ma (Fig. 2). Four samples were taken representing chronostratigraphic levels between 18·9 Ma and 13·6 Ma. A further sample, still belonging to the lower sedimentary cycle (USM), was taken from the Fischenbach section ≈ 15 km further to the east representing an age of 20·9 Ma (Schlunegger *et al.*, 1996).

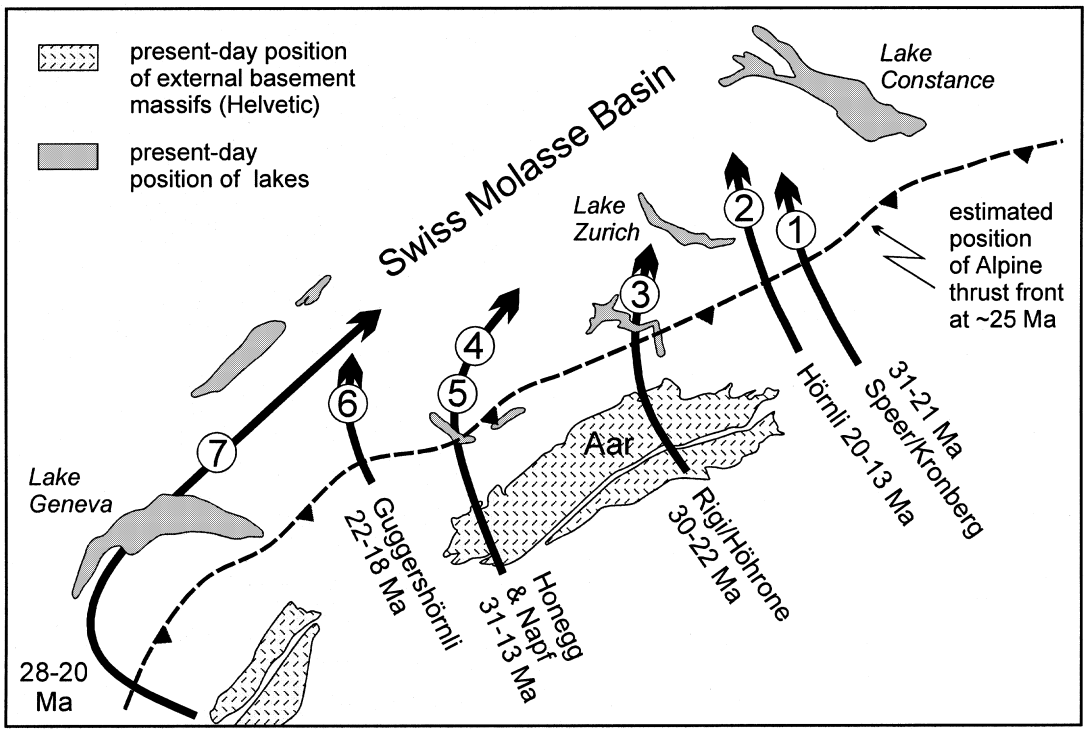

Fig. 3. Palaeodrainage map showing present-day position of external basement massifs, lakes and investigated sections as well as the estimated position of the Alpine thrust front in late Oligocene times. Arrows indicate drainage directions of palaeorivers (modified after Schlunegger *et al.*, 1998; Kuhlemann & Kempf, 2002). Numbers correspond to Figs 1 and 2.

(5) Honegg alluvial fan system

The Rupelian to latest Chattian/earliest Aquitanian deposits of the transverse Honegg palaeoriver in the area east of Lake Thun (≈ 30 km SE of Berne) largely reflect the period of the first regressive megacycle in the SMB, and are composed of three major coarsening-upward cycles ranging from flood plain deposits to massive alluvial fan conglomerates (Schlunegger *et al.*, 1996). Six samples were taken representing chronostratigraphic levels between 31·0 Ma and 24·0 Ma (Schlunegger *et al.*, 1996).

(6) Guggershörnli fan and Seftigschwand thrust sheet

The Heitenried/Sensegraben/Guggershörnli section 20 km south-west of Berne exhibits a Burdigalian coarsening-upward sequence from marine tidal flat to fan delta to alluvial fan deposits. The onset of the progradation of the Guggershörnli alluvial fan is dated at 18·6 ± 0·2 Ma (Strunck, 2001), which probably formed in response to the thrusting of the northernmost thrust sheets of the SMB (Seftigschwand). The latter is exposed about 10 km to the east and is composed of Aquitanian flood plain deposits that show a general coarsening-upward trend, indicating a shift from more distal to more proximal conditions (Strunck, 2001). Six samples were taken representing chronostratigraphic levels between 22·5 Ma and 17·9 Ma (Strunck, 2001).

(7) Lake Geneva axial drainage system

The Lake Geneva drainage system is the only axial drainage considered in this study because of its strong influence on the entire Chattian to Aquitanian fluvial system running parallel with the axis of the SMB and draining from south-west to north-east. In the western SMB, it covers the whole area belonging to the present-day undeformed Plateau Molasse and also some parts of the folded/thrusted Subalpine Molasse (Maurer, 1983). The entry point of the detrital material into the foreland basin is not known exactly but must have been located to the south or south-west of present-day Lake Geneva. Four samples were taken representing chronostratigraphic levels between 28·1 Ma and 23·9 Ma (Strunck, 2001).

ANALYTICAL METHODS

Whenever possible, sampling concentrated on unweathered fine- to medium-grained sandstones (Table 1). Light mineral data were obtained by counting at least 300 points in thin section. Thin sections were stained for easy identification of calcite and to distinguish it from dolomite. In contrast to the Gazzi–Dickinson method (Ingersoll *et al.*, 1984), minerals >63 μm within lithoclasts were counted as the type of lithoclast in which they occur (Decker & Helmold, 1985; Johnsson *et al.*, 1991; von Eynatten & Gaupp, 1999). Percentage raw data and calculated framework parameters are listed in *Supplementary material*, Table S1. No point-count data were obtained from sample EY 21-9 because of its very fine grain size. Table 2 gives a brief description of individual grain types.

For heavy mineral analysis, samples were crushed to sizes <4 mm and subsequently disaggregated in 10% acetic acid at 60–70 °C to remove carbonate cement. Heavy minerals were obtained from the 63–125 μm sieve fraction of the disaggregated sand by centrifuge-aided settling in Na-metatungstate (calibrated density 2·88 ± 0·02 g cm^{-3}). The small grain size minimizes the grain-size effect on heavy mineral counts (Morton & Hallsworth, 1994) and, in particular, the strong grain size-related bias introduced by the high garnet content of Swiss Molasse deposits (e.g. Füchtbauer, 1964). Generally, 200 non-opaque, non-micaceous, non-carbonate minerals were counted using the ribbon-counting method (Mange & Maurer, 1991). The following major species or groups of heavy minerals were distinguished (*Supplementary material*, Table S2): zircon (zrn), tourmaline (tur), rutile and other TiO_2 minerals (rt), garnet (grt), epidote group minerals (epi), apatite (ap), staurolite (st), chrome spinel (chr), blue sodic amphibole (gln) and others. The last category includes titanite, sillimanite, kyanite, chloritoid, monazite/xenotime, pyroxene, pumpellyite, hornblende and tremolite.

Whole-rock chemical compositions of powdered samples (corundum ball mill) were obtained running standard X-ray fluorescence (XRF) routines on a Philips PW 2400 wavelength-dispersive spectrometer system using a Rh tube. Major elements were measured on fused discs, and trace elements were measured on pressed powder pellets (Rollinson, 1993). Relative errors on major and trace elements are usually <2% and 5% respectively. Loss on ignition (LOI) was determined by heating the dried samples to 950 °C for 2 h. Total iron is expressed as Fe_2O_3. Chemical data are listed in *Supplementary material*, Table S3.

Table 2. Description of grain types.

Q_m	Monocrystalline quartz grains
Q_p	Polycrystalline quartz grains
Q_c	Chert: micro- to cryptocrystalline quartz grains, sometimes relics of radiolaria are recognized
D	Dolomite grains: range from fine-grained dolosiltite to coarse-grained single detrital dolomite crystals
C_m	Micritic calcite grains: prone to show recrystallization during diagenesis (compaction and calcite precipitation) of the sandstones
C_s	Sparitic calcite grain: only detectable when original grain boundaries were preserved, otherwise the possible former calcite grain was counted as authigenic calcite (C_{aut})
F	Feldspar grains: mostly quite fresh, but some strongly altered (sericitized, kaolinized), no differentiation was made between K-feldspar and plagioclase
L_{sm}	Quartz–chlorite–mica aggregates: foliated clasts of quartz and sheet silicates, some showing solution precipitation creep typical of low-grade rocks, most probably metasediments
L_s	Non-carbonate sedimentary lithoclasts: some shales but mostly siltstones to fine-grained sandstones, partly showing illite and/or chlorite formation but sedimentary textures are still preserved
L_{qf}	Quartz–feldspar aggregates: intergrowth of quartz and feldspar, some perthitic and myrmekitic textures, rarely mica or chlorite may be present, generally no metamorphic textures
L_v	Volcanic lithoclasts, usually basic or intermediate: fine-grained matrix with mostly altered feldspar phenocrysts
L_u	Ultrabasic lithoclasts: serpentinite fragments
m	Mica
chl	Chlorite
hm	Heavy minerals (for specification, see Supplementary material, Table S2)
gla	Glauconite

RESULTS

Sandstone framework composition (light minerals)

According to the first-order classification of arenites by Zuffa (1980), all samples are sandstones, which means that they are composed almost exclusively of non-carbonate and carbonate extraclasts. According to the second-order classification scheme of McBride (1963), the majority of sandstones are litharenites or feldspathic litharenites, but some are lithic subarkoses or lithic arkoses (Fig. 4).

The total carbonate content (C_t) of all samples based on point-count data varies between 11% and 81% with authigenic carbonate (C_{aut}) ranging between 10% and 35% (*Supplementary material*, Table S1). Detrital carbonate grains range from 2% to 59% with dolomite clasts being the major constituent (up to 49%). Total quartz content (Q_t) varies between 14% and 49%. The third major component of the sandstones is feldspar, which occurs either as single fragments (0·3–27%) or within quartz–feldspar aggregates (L_{qf}, 0–29%). Minor components that are important in some locations are quartz–chlorite–mica aggregates (L_{sm}, up to 16%), serpentinite fragments (L_u, up to 9%) and mafic to intermediate volcanic lithoclasts (L_v, up to 8%).

Based on their significance as specific source-rock indicators, individual clast types were grouped together to calculate sandstone framework parameters. The resulting data were used to demonstrate the evolution of sandstone composition in response to changing source-rock units in space and time (Fig. 5). Key parameters are: $S = \text{sum}(Q_c, D, C_m, L_s)$, $G = \text{sum}(F, L_{qf})$, $M = L_{sm}$ and $O = \text{sum}(L_u, L_v)$ (*Supplementary material*, Table S1). Parameter S is considered to reflect the erosion of sedimentary rocks of Austroalpine and/or Penninic origin. Such sources are largely composed of carbonates (D, C_m), radiolarites (Q_c) and flysch-like sediments (L_s). Parameter G is considered to reflect erosion of granitoid to gneissic source rocks from crystalline basement nappes of Austroalpine and/or Penninic origin, whereas parameter M reflects the exposure of low-grade metamorphic rocks, most probably of Penninic origin. Finally, parameter O is considered to reflect ultramafic to mafic/intermediate source rocks, which, in the case of a significant contribution of serpentinite (L_u), originate from Penninic ophiolitic units.

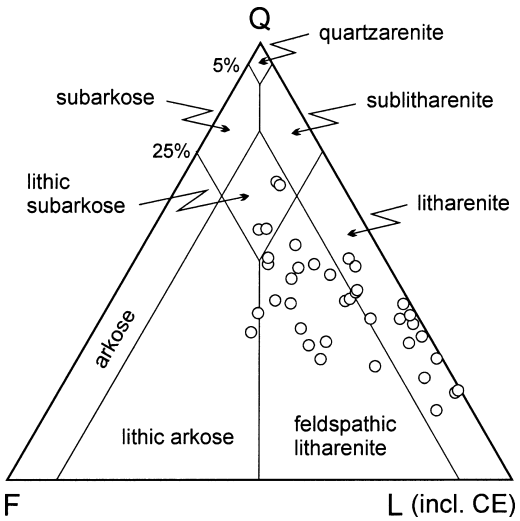

Fig. 4. Classification of sandstones based on framework composition (McBride, 1963). Carbonate extraclasts (CE) are included in the L-pole. The majority of sandstones are (feldspathic) litharenites.

Variations in sandstone framework parameters in space and time are shown in Fig. 5. To summarize, the most prominent characteristics are:

1 the predominance of sedimentary source rocks in the eastern part of the SMB (Sections 1 and 2) throughout the studied stratigraphic column, as well as in the more central Section 3 up to ≈25 Ma;

2 the abrupt change at ≈25 Ma in Section 3 from predominantly sedimentary source rocks to granitoids, which is also observed in the more westerly Section 5. In the westernmost Sections 6 and 7, granitoid sources generally predominate over sedimentary sources except for the youngest deposits at ≈18 Ma;

3 a strong decrease in granitoid-derived detritus at ≈20 Ma in Sections 4 and 6, partly replaced by a significant contribution from low-grade metasediments, which persists up to the youngest deposits at ≈13 Ma;

4 a significant contribution from ultramafic rocks and mafic volcanics to 28–27 Ma sandstones in the westernmost Section 7 and to sandstones younger than 21 my in the east (Section 2). Some mafic to intermediate volcanics also contribute to the central Sections 4 and 5, but no ultramafic sources are recognized in this part.

Geochemistry

Chemical data are used to constrain source-rock variations in space and time by applying chemical proxies that best reflect the contribution of

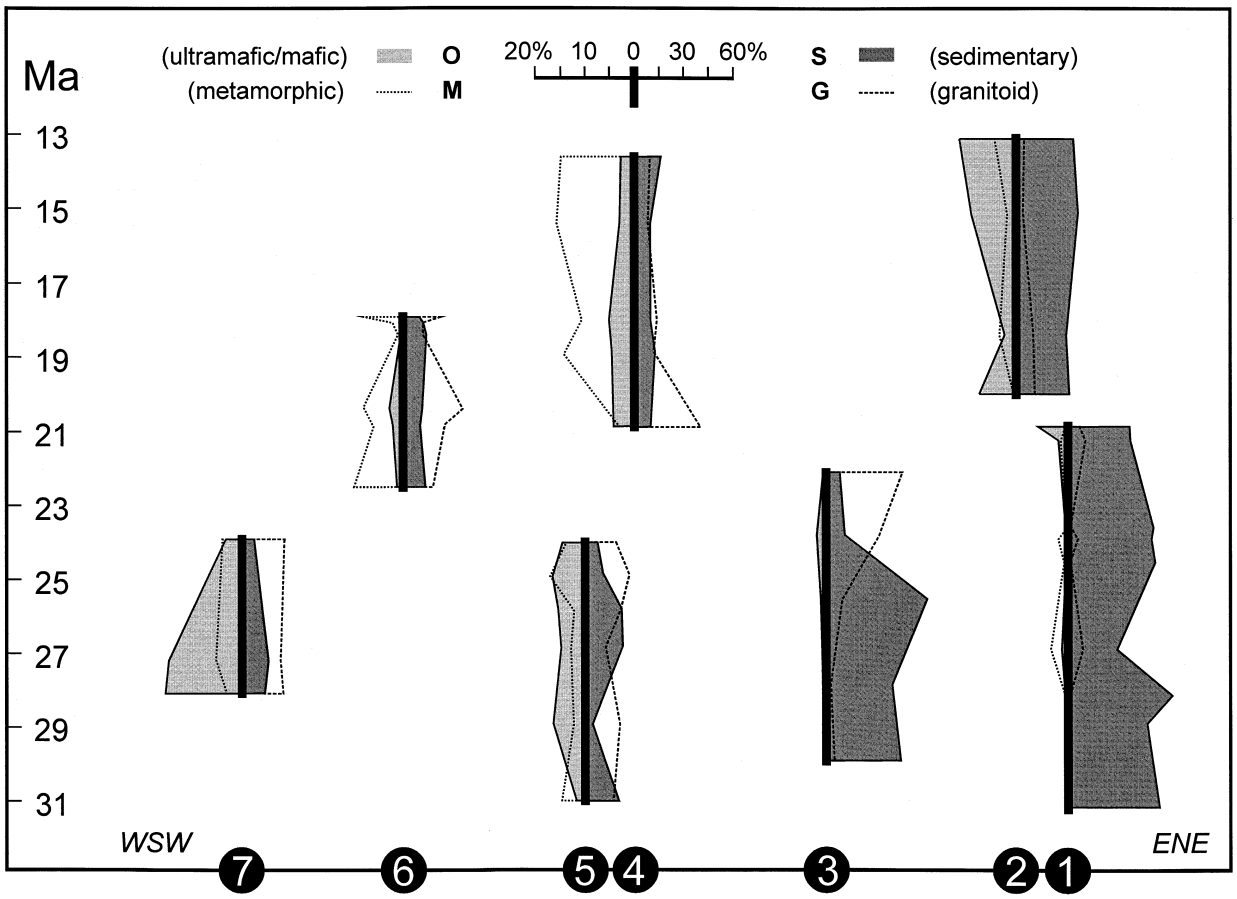

Fig. 5. Variations in light mineral framework parameters S (sedimentary sources), G (granitoid sources), M (low-grade metasedimentary sources) and O (mafic to ultramafic sources) in space and time. Scale at top refers to all sections. For locations and sedimentary sequences, compare Figs 1 and 2.

specific source-rock lithologies. Primarily, major elements and LOI reflect the large range of mixing between silica/silicate phases and carbonate phases in the sandstones. SiO_2 and CaO are negatively correlated (Fig. 6) and range from 25% to 73% and from 55% down to 7% respectively (*Supplementary material*, Table S3). CaO is largely derived from carbonates given the strong positive correlation between CaO and LOI (Fig. 6), which results from the breakdown of $CaCO_3$ to CaO and CO_2 (included in LOI) during fusion of the sample. High MgO contents (up to 18%) appear to be largely derived from dolomite given the positive correlation between MgO and CaO, and MgO and LOI (Fig. 6). Also, MgO may be derived in part from ultramafic and mafic volcanic clasts. The calculated average contribution of MgO from (ultra)mafics to the measured total MgO based on light mineral data is $<0{\cdot}5\%$. This suggests that MgO is mainly an indicator of detrital dolomite in the sandstones. Consequently, the MgO/SiO_2 ratio can be used as a chemical proxy indicative of a sedimentary source. This assumption is corroborated by a significant negative correlation of G/S ratios from light mineral data and MgO/SiO_2 ratios (Fig. 7).

Significant positive correlation is observed between G/S ratios and Na_2O/SiO_2 ratios (Fig. 7), a relationship that implies that the latter ratio is indicative of feldspar-rich granitoid sources (G). This argument is strengthened by the general dominance of Na-rich plagioclase compared with K-feldspar (Füchtbauer, 1964). The observed variations in Na_2O/SiO_2 and MgO/SiO_2 ratios (Fig. 8) show a similar pattern compared with the variation in G and S contents based on light mineral data (Fig. 5). This similarity includes:

1 the strong contribution of sedimentary source rocks in the eastern sections and the slight increase in granitoid sources in these sections between ≈ 22 and ≈ 18 Ma;

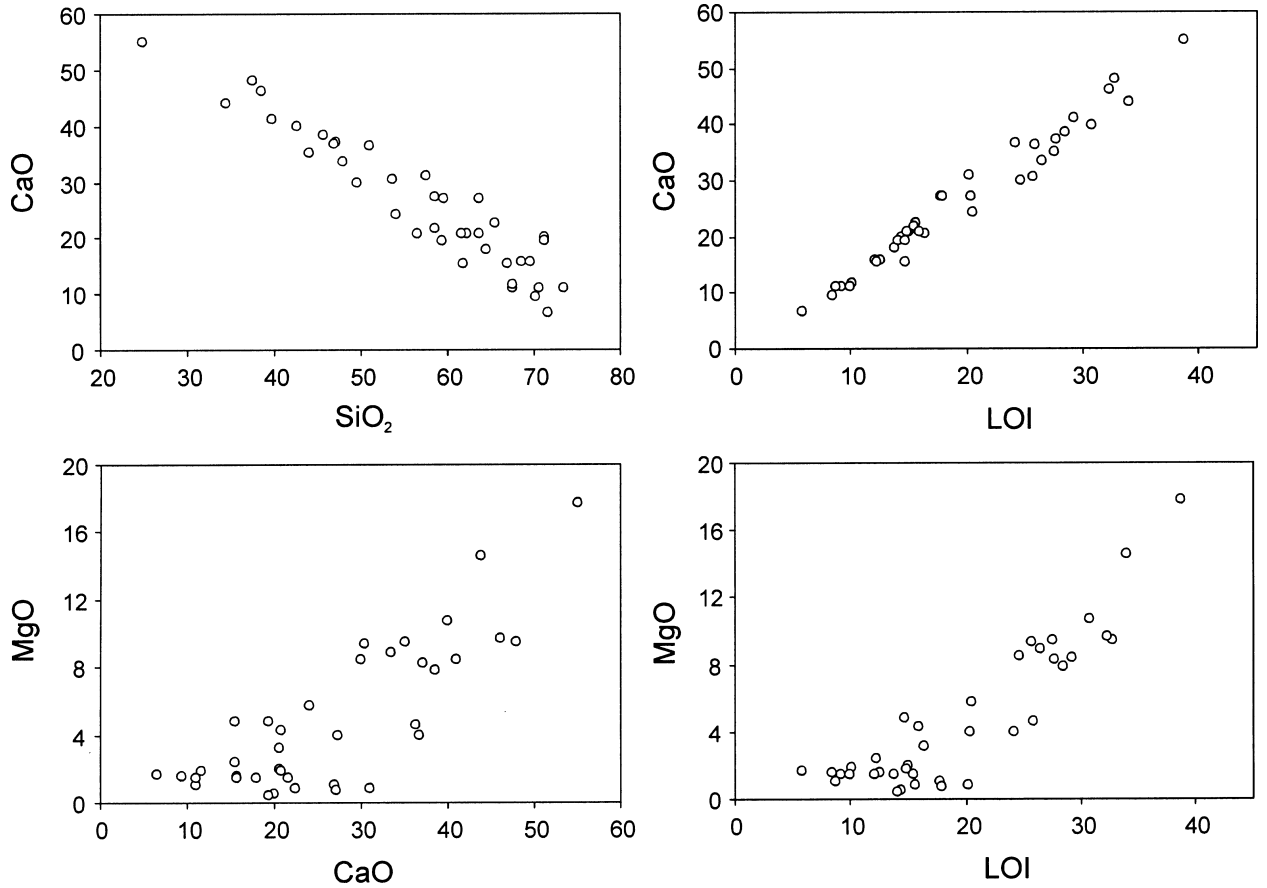

Fig. 6. Bivariate variation diagrams for major element oxides CaO, SiO_2, MgO, Na_2O, Al_2O_3 and loss on ignition (LOI).

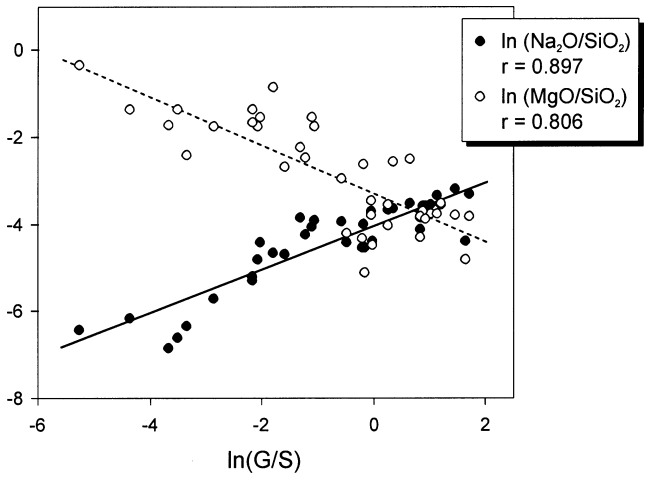

Fig. 7. Log-ratio correlation diagram showing the two major element ratios MgO/SiO_2 and Na_2O/SiO_2 compared with the ratio of granitoid (G) to sedimentary (S) sandstone clasts. Both chemical proxies correlate highly significantly (at the 99% confidence level) with the G/S ratios and are therefore considered to provide useful estimates of the relative contribution of granitoid and sedimentary source rocks.

2 the abrupt change in the dominant source lithology at ≈25 Ma from sedimentary rocks to granitoids in Section 3; and

3 the predominance of granitoids in the western (starting at the base of Section 7) and central source areas (starting at ≈26 Ma in Section 5), which lasted up to ≈20 Ma (Sections 6 and 4).

Major elements provide no reasonable indicators of (ultra)mafic sources, but Cr and Ni can be used to evaluate their influence (Garver *et al.*, 1996). Cr/Ba and Ni/Ba ratios appear to reflect, quite precisely, the contribution from such sources. In this context, Ba is thought to monitor the contribution of felsic crystalline rocks, an

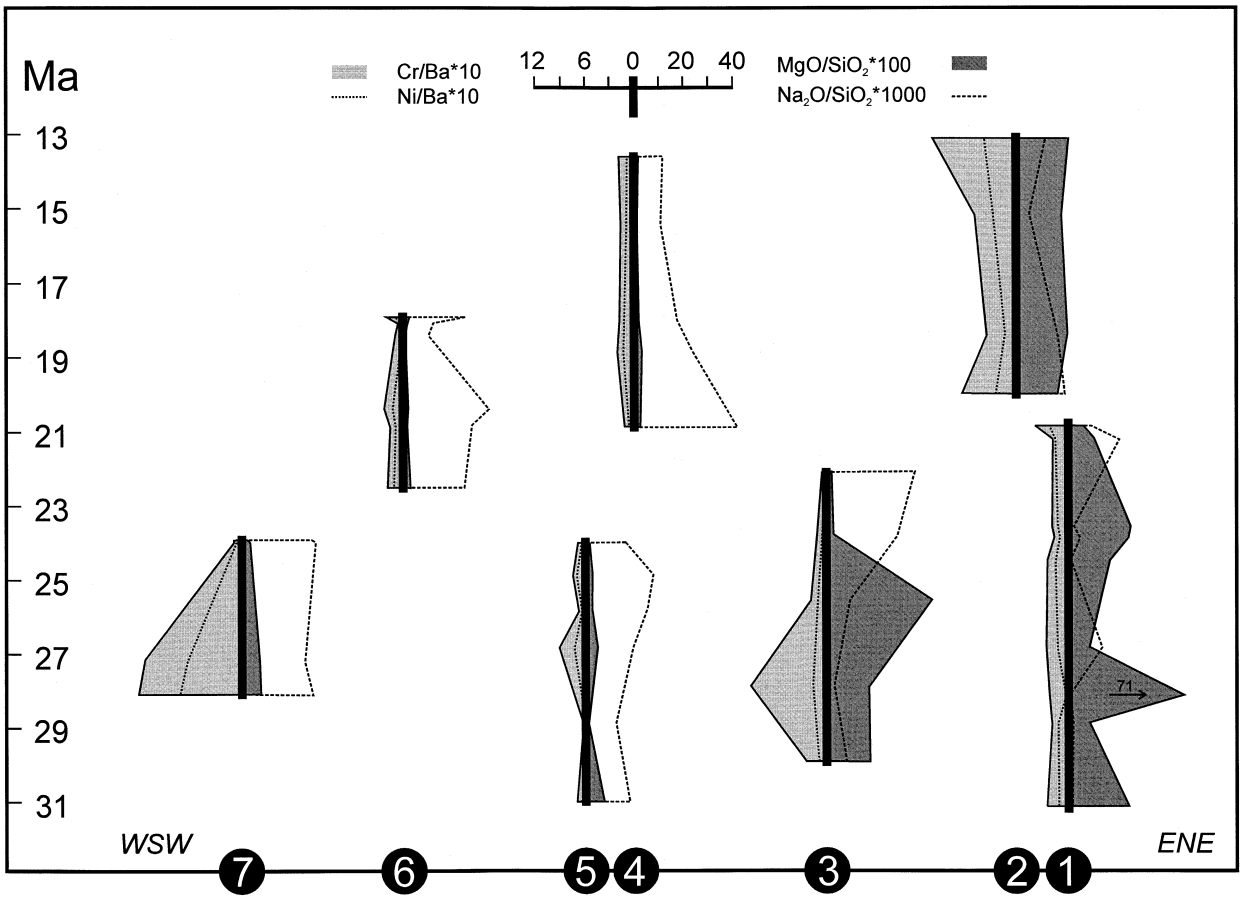

Fig. 8. Variations in chemical proxies MgO/SiO_2, Na_2O/SiO_2, Cr/Ni and Ba/Ni in space and time. For locations and sedimentary sequences, refer to Figs 1 and 2. Note the similarity of patterns compared with Fig. 5 and the similar relative behaviour of Cr/Ba and Ni/Ba except for samples EY 18-3 (≈ 28 Ma in Section 3) and EY 19-10 (≈ 28 Ma in Section 1).

assumption that is supported by a positive correlation between feldspar and Ba contents of the sandstones. The pattern of Cr/Ba and Ni/Ba ratios (Fig. 8) shows strong similarities compared with the pattern of the framework parameter O indicative of (ultra)mafic sources (Fig. 5). The only inconsistency is the high Cr/Ba ratio in sample EY 18-3 (≈ 28 Ma in Section 3), which does not correspond to its low Ni/Ba ratio and negligible content of (ultra)mafic lithoclasts. This discrepancy points to contrasting sources for Cr and Ni in at least some sediments and will be discussed later together with the origin of detrital chrome spinel.

Chemical data do not provide a reasonable proxy for estimating the contribution from low-grade metasedimentary source rocks (M, Section 4), because such clasts are composed essentially of quartz and sheet silicates that do not yield a unique chemical signal for estimating their amount in the sandstones.

Heavy minerals

The main heavy mineral species in the studied sections are epidote group minerals (up to 90%), garnet (up to 80%), apatite (up to 48%) and the ultrastable zircon, tourmaline and rutile (ZTR, up to 61%), as shown in previous studies (von Moos, 1935; Füchtbauer, 1964; Matter, 1964; Mange-Rajetzky & Oberhänsli, 1982; Maurer, 1983; Schlunegger *et al.*, 1993; Kempf *et al.*, 1999). Other heavy minerals of local importance are staurolite, chrome spinel and blue sodic amphibole. Variations in heavy minerals in space and time are displayed in Fig. 9.

Sandstones older than ≈21 Ma from the more easterly Sections 1 and 3 are characterized by a high garnet content (up to 75%) as well as zircon, tourmaline and rutile (ZTR, up to 40%; *Supplementary material*, Table S2). Higher amounts of chrome spinel (up to 31%) appear to be associated with high amounts of ZTR (Fig. 9). Occasionally,

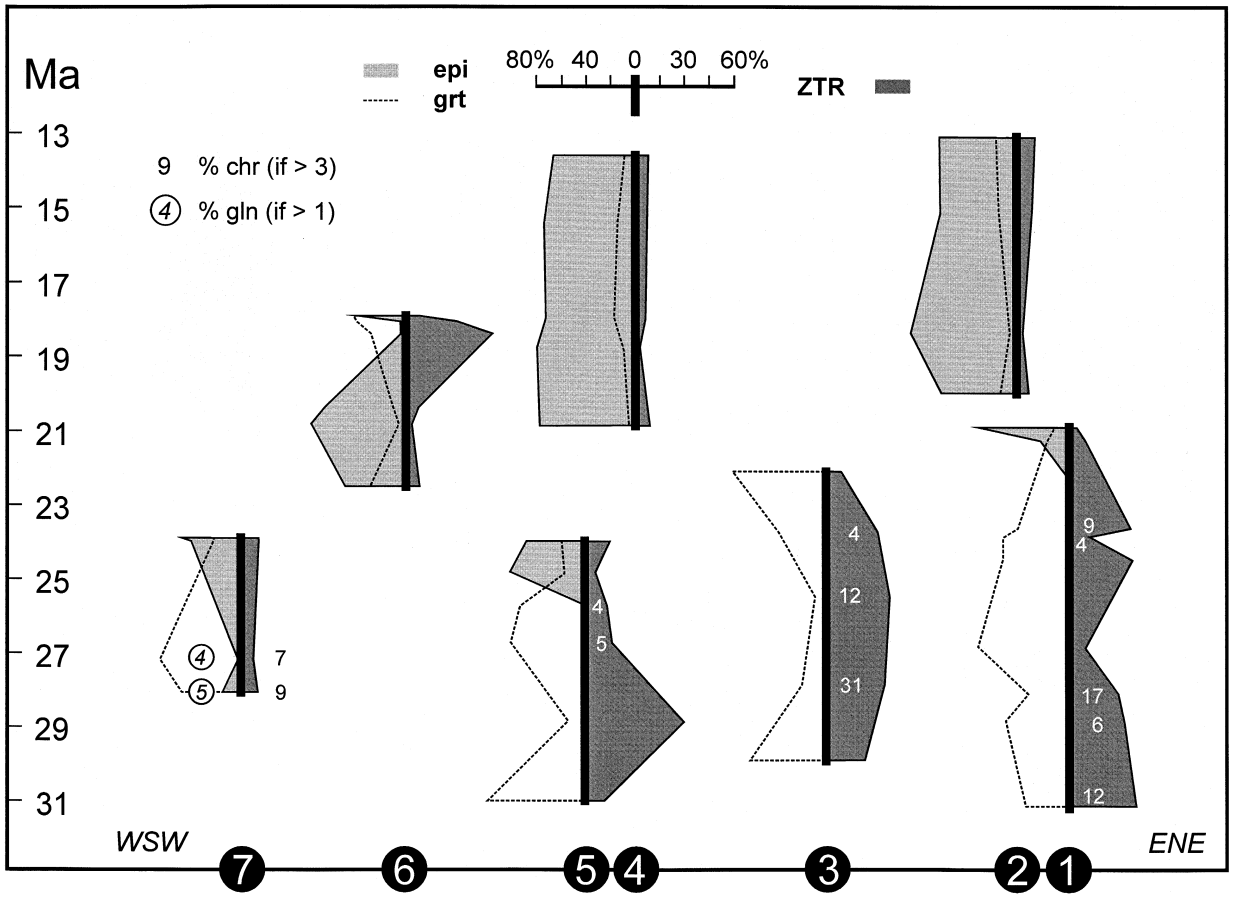

Fig. 9. Variations in heavy minerals (epi, epidote; grt, garnet; ZTR, zircon + tourmaline + rutile) in space and time. For locations and sedimentary sequences, see Figs 1 and 2. Numbers indicate percentage of chrome spinel (chr) and blue sodic amphibole (gln).

apatite becomes an important constituent (up to 48%), and staurolite content may exceed 20%. At ≈21 Ma, a major change in the heavy mineral spectra is observed in the eastern sections when epidote becomes the dominant heavy mineral (up to 90%). Garnet and ZTR decrease dramatically, chrome spinel and staurolite are low (≤ 1·5% and ≤3·0% respectively). This pattern persists up to the top of Section 2 at ≈13 Ma.

In the central Sections 4 and 5, sediments older than 25 Ma are more or less similar in their heavy mineral composition compared with the eastern sections. Chrome spinel is always present (up to 5%), staurolite was observed in only one sample, and epidote is virtually absent. At ≈25 Ma, epidote becomes predominant (up to 80%). Garnet, ZTR and apatite decrease, and chrome spinel disappears from samples younger than 25 Ma This pattern persists up to the top of Section 4 at ≈13·6 Ma.

In the westernmost Section 7, the oldest deposits (≈ 28 Ma to ≈27 Ma) show high garnet contents (48–66%) and relatively low contents of ZTR (≈ 10%), epidote (≤ 16%) and apatite (≤ 13%). Important characteristics are significant amounts of chrome spinel (> 6%) and blue sodic amphibole (> 3%, Fig. 9). The latter is regarded as a key heavy mineral for the Chattian Lake Geneva dispersal system (Maurer, 1983). Higher up in Sections 7 and 6, at ≈24 to ≈20 Ma, epidote increases (41–77%), whereas garnet decreases (4–29%) and ZTR remains low (4–11%). Chrome spinel and blue sodic amphibole are no longer present. In Section 6, at ≈18 Ma (Guggershörnli alluvial fan), contrasting heavy mineral spectra were observed that are mostly characterized by high ZTR contents and reoccurrence of some chrome spinel grains.

Summarizing the variation in heavy mineral spectra, the most prominent characteristics are:

1 a major shift from garnet- and/or ZTR-dominated heavy mineral spectra to epidote-rich heavy mineral spectra at ≈21 Ma in the eastern sections. This change occurs ≈4 Ma earlier in the central and western sections (Fig. 9); and

2 high chrome spinel contents (up to 31%) are largely concentrated in the older sediments of Sections 1 and 3 and appear to be associated with abundant ZTR. An exception is the frequent occurrence of chrome spinel in the oldest parts of Section 7, which is associated with significant proportions of blue sodic amphibole.

DISCUSSION

Sandstone composition, alteration and grain size

Sandstone framework parameters S (sedimentary rock fragments), G (feldspars and felsic plutonic fragments), M (metasedimentary rock fragments) and O (ultramafic to intermediate volcanic rock fragments) do not reflect quantitatively the eroded volumes of their source rocks because most of these rocks also contribute in contrasting amounts to the quartzose grain types Q_m and Q_p. In addition, the resistance of the individual grain types to physical and chemical abrasion during weathering, transport, deposition and diagenesis must be considered (e.g. Johnsson, 1993).

The effects of changes in sandstone composition as a result of chemical or mechanical alteration appear to be quite low, as indicated by the high amount of lithoclasts (Grantham & Velbel, 1988; Weltje *et al.*, 1998; Fig. 10). Among the latter, carbonate clasts are most sensitive to dissolution, and their high frequency underlines the low degree of modification of the original sources. This is supported by the frequency of relatively fresh feldspar (Füchtbauer, 1967). Because coarse-grained proximal sediments of the Molasse basin of Switzerland show very little modification of sandstone composition by weathering and/or diagenesis, framework parameters do provide robust estimates of the relative variations of the eroded source rocks. The low degree of overall alteration also permits the use of chemical proxies (e.g. the Na_2O/SiO_2 ratio) as a measure for the contribution of feldspar-rich granitoid source rocks.

In this context, the influence of grain size on sandstone composition should be evaluated briefly. Figure 11 illustrates that neither sandstone framework parameters (G/S ratios as an example) nor the chemical proxies (Na/Si, Mg/Si and Ni/Ba) used to estimate relative contributions of prominent source rocks vary systematically with grain size. There is also no correlation between grain size and age or location of samples. Similar conclusions were drawn from a study of chrome spinel concentrations in Swiss Molasse sandstones by Gasser (1968).

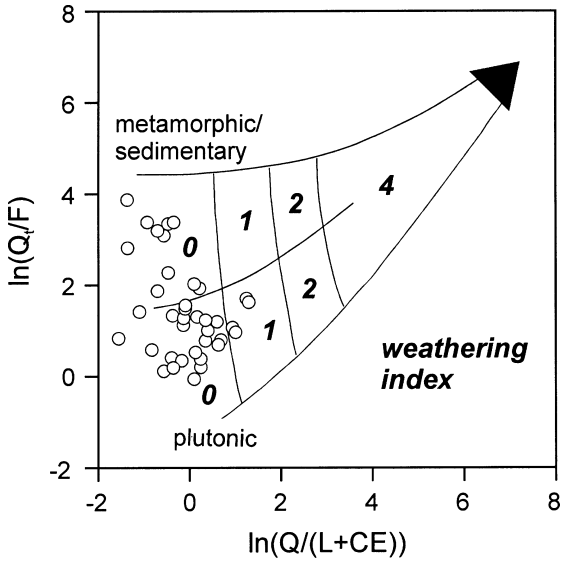

Fig. 10. Bivariate log-ratio diagram $\ln(Q_t/F)$ vs. $\ln[Q/(L + CE)]$ suggesting very low weathering of the sandstones (modified after Weltje *et al.*, 1998). Weathering indices range from 0 (unweathered) to 4 (intensely weathered). An index of 0 requires either (semi-)arid conditions or a high mountainous relief. The latter is supposed for the Oligocene to Miocene Central Alps.

The source of chrome spinel

Inconsistencies between Cr/Ba and Ni/Ba ratios suggest contrasting sources for Cr and Ni in some of the sediments as mentioned above. The main potential carriers of Cr and Ni are serpentinite fragments, chrome spinel and mafic volcanic lithoclasts. Samples with high chrome spinel contents (chr > 5%) are mostly free of serpentinite (L_u, group I in Fig. 12A), and samples with a significant contribution of $L_u \geq 2\%$ are very low in chrome spinel (group II), suggesting that serpentinite fragments and chrome spinel are essentially not related.

Only the two samples with the highest values of L_u ($\approx 9\%$) show elevated concentrations of chrome spinel, reaching 9% (group III, Fig. 12A). These samples show Cr/Ni ratios typical of ultramafic rocks (Fig. 12B). Cr/Ni ratios of group II samples are slightly higher up to $\approx 2{\cdot}8$ but still in the range of Penninic metabasalts (Pfeifer *et al.*, 1989; Frisch *et al.*, 1994). In contrast, Cr/Ni ratios of group I samples range up to ≈ 16. Such high ratios suggest the occurrence of chrome

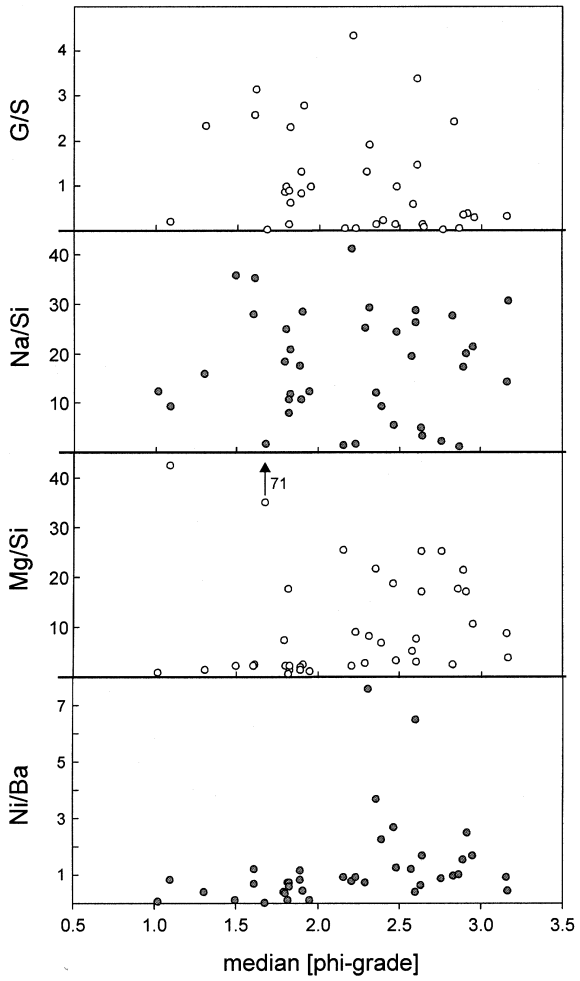

Fig. 11. Bivariate plots of grain size (median) vs. sandstone framework parameters (G/S) and chemical proxies (Na/Si, Mg/Si and Ni/Ba) showing no systematic variation in sandstone composition and grain size for the analysed fine- to medium-grained sandstones.

spinel but a very low abundance of serpentinite and mafic volcanics. This may be explained by either extensive sorting or recycling, which concentrates chrome spinel relative to unstable serpentinite and volcanic clasts. The latter interpretation is supported by the fact that group I samples have abundant sedimentary rock fragments and high concentrations of the ultrastable heavy minerals (ZTR ≥ 30). Potential sources for the recycled chrome spinel are Cretaceous Austroalpine siliciclastics or Penninic flysch units (Gasser, 1967; Gaupp, 1980; von Eynatten, 1996).

The interpretation that (1) chrome spinels in group I samples were derived from recycling of chrome spinel-bearing sediments and (2) chrome spinels in group II and III samples are first-cycle minerals from (ultra)mafic rocks is corroborated by the composition of the detrital chrome spinels (Fig. 13). Chrome spinel compositions from group I samples (Section 1 at 28 Ma) are similar to those from Cretaceous siliciclastics, whereas chrome spinel in samples from groups II (Section 2 at 13 Ma) and III (Section 7 at 28 Ma) are different in composition and indicate derivation from mid-ocean ridge (MORB) and intraplate basalts (IPB). Such rocks are presently exposed in the Penninic Arosa and Zermatt-Saas zones (Fig. 1).

The source of epidote group minerals

Füchtbauer (1964) concluded that epidote group minerals in the Swiss Molasse were derived from either Penninic metabasaltic rocks ('greenstones') or from Penninic and/or Austroalpine metagranitoids. In the eastern part of the SMB, the abrupt appearance of epidote in sediments at ≈ 21 Ma coincides precisely with the increase in (ultra)mafic lithoclasts and Cr/Ba ratios, and not with an earlier increase in granitoid clasts and Na_2O/SiO_2 ratios (Figs 8 and 9). Consequently, epidote in the eastern sections most likely derived from the same Penninic metabasalts that delivered the detrital chrome spinel (group II, see above). A similar observation was made by Kempf *et al.* (1999) using heavy mineral data and conglomerate-clast compositions. In the central part of the basin, the abrupt appearance of epidote at ≈ 25 Ma coincides with an increase in granitoid clasts and Na_2O/SiO_2 ratios. A contemporaneous increase in granite pebbles within conglomerate clasts was recorded by Schlunegger *et al.* (1993), thus supporting the interpretation that epidote in the central part is derived from (meta)granitoid rocks.

These conclusions are corroborated by Nd and Sr isotopic data from the epidote grains, suggesting mantle-derived sources for the eastern epidotes and largely crustal sources for the central epidotes (Spiegel *et al.*, 2002). In the west, the situation is less clear, because epidote is present in stratigraphic levels where both (ultra)mafic and granitoid sources contributed detritus. However, the highest concentrations of epidote coincide with the highest concentrations of granitoid clasts and highest Na_2O/SiO_2 ratios (Figs 5, 8 and 9), suggesting a predominance of crust-derived sources for epidote in the western sections.

Space–time framework of eroded source rocks

A summary of the petrographic and geochemical results is given in Fig. 14 showing relative proportions of the different source rocks contributing

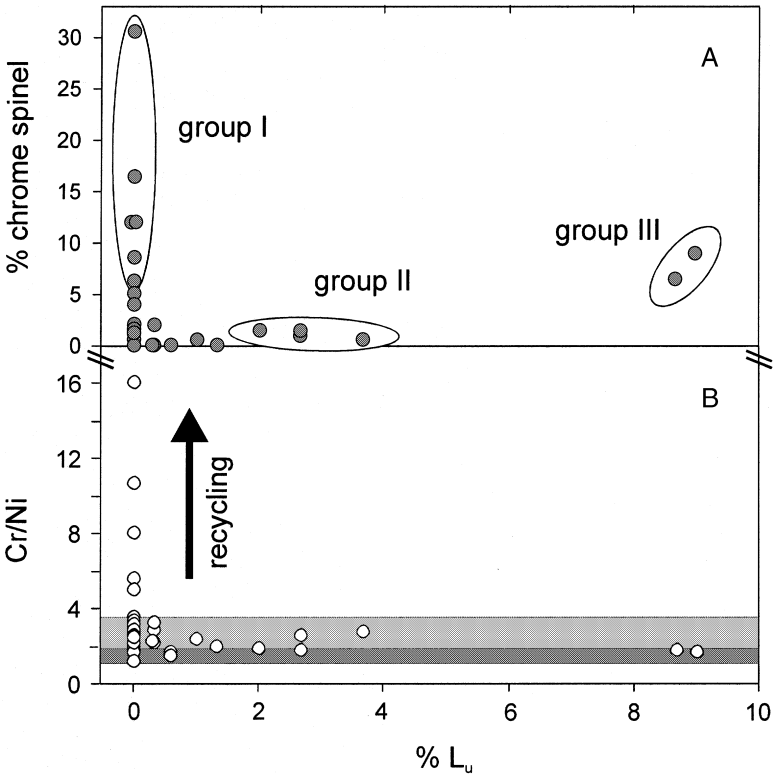

Fig. 12. Bivariate plots of percentage serpentinite fragments (L_u) vs. percentage chrome spinel in heavy mineral spectra (A) and Cr/Ni ratios (B). Group I samples are from the lower parts of Sections 1 and 3, group II samples from Sections 1 and 2 younger than ≈ 21 Ma, and group III samples are from the base of Section 7. Dark grey field indicates Cr/Ni ratios between 1·2 and 1·9, typical of ultramafic rocks (Hyndman, 1985; Garver *et al.*, 1996) and, specifically, of Penninic ultramafic rocks from the Arosa zone (Frisch *et al.*, 1994) and the Zermatt-Saas zone (Pfeifer *et al.*, 1989). Light grey field reaches up to Cr/Ni = 3·5 as determined from Penninic metabasalts (Pfeifer *et al.*, 1989; Frisch *et al.*, 1994).

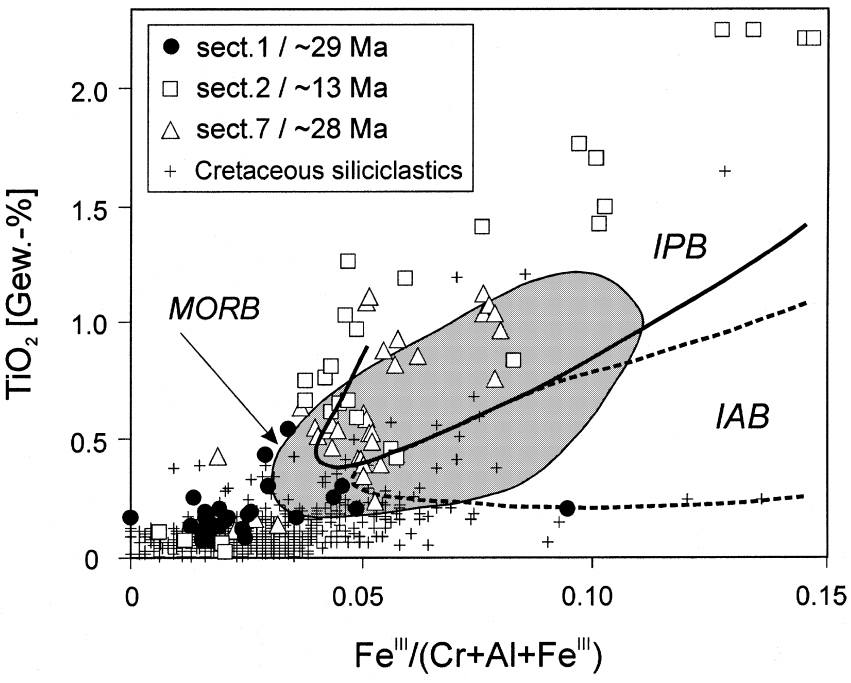

Fig. 13. Plot of TiO_2 vs. Fe^{III} number from microprobe data of detrital chrome spinels. Ferric iron was calculated assuming mineral stoichiometry. Compositional fields of chrome spinel from mid-ocean ridge (MORB), intraplate (IPB) and island-arc basalts (IAB) were taken from Arai (1992). Crosses indicate compositions of > 500 single chrome spinels from Cretaceous flysch-like siliciclastics (von Eynatten, 1996); the other symbols represent chrome spinel composition from samples from Swiss Molasse sandstones. Chrome spinel chemistry was determined on polished heavy mineral separates with a Jeol JXA 8900 RL electron microprobe at the University of Göttingen applying the wavelength dispersive method.

to the bulk composition of Oligocene to Miocene Swiss Molasse sandstones. These proportions are largely based on sandstone framework parameters and whole-rock geochemistry, with additional constraints from heavy mineral analysis and mineral chemistry. The space–time framework of source rocks shows four major breaks (solid lines in Fig. 14). The horizontal lines indicate breaks in time and the subvertical line a break in space. Further breaks are marked by dashed lines.

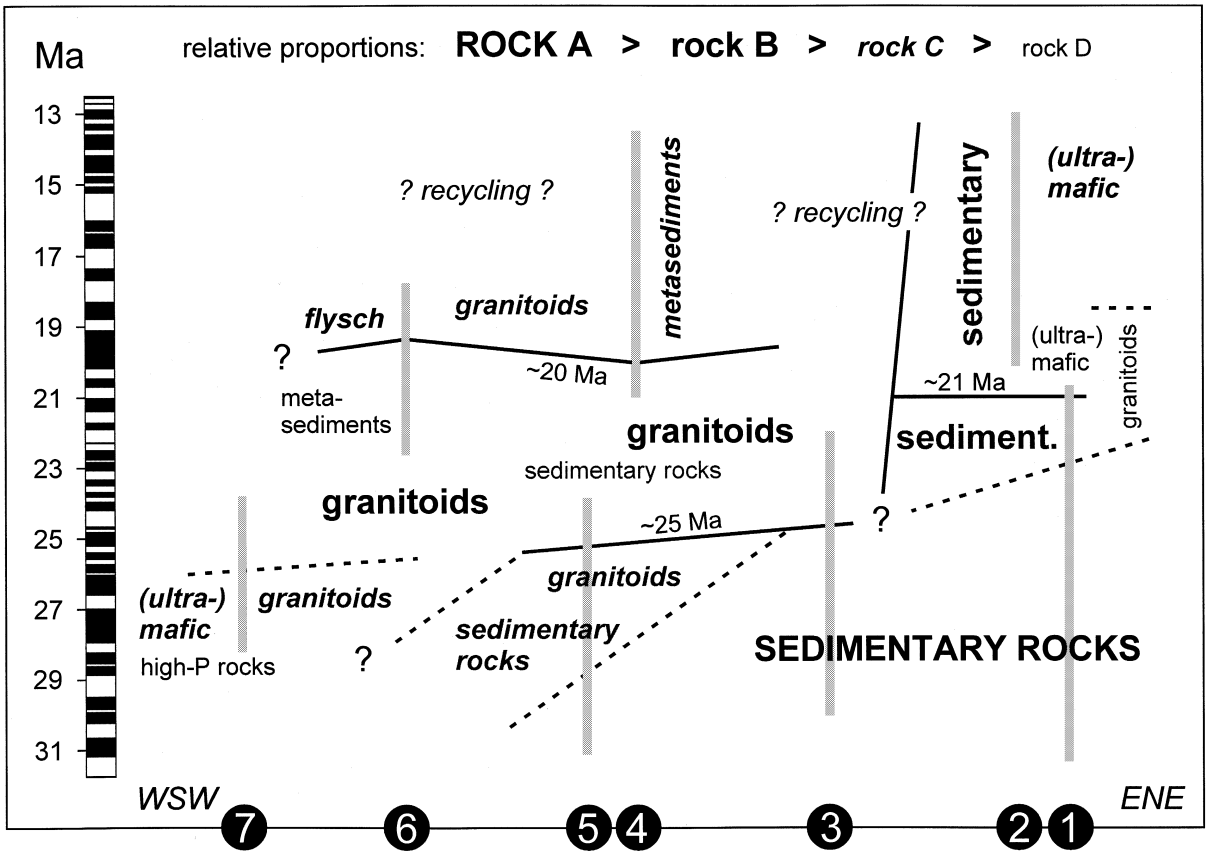

Fig. 14. Space–time framework of eroded source rock lithologies. Size and style of rock name indicate relative proportions of the contribution of the specified rock type to the bulk composition of sandstones. Grey bars indicate stratigraphic range of Sections 1–7 (Fig. 2). Solid black lines indicate major breaks in source rock lithology, stippled lines indicate minor breaks or stratigraphically less constrained changes. Recycling of older Molasse strata must be considered but is difficult to quantify.

These are either less important or stratigraphically less well constrained.

The main spatial break separates the eastern part (Sections 1 and 2) between ≈25 Ma and ≈13 Ma from the rest of the basin and, consequently, the eastern source areas from the central and western sources. This separation is based on the predominance of sedimentary lithic fragments throughout the stratigraphic column in the eastern sections. The sedimentary sources are mostly dolomitic but also include micritic limestones, flysch-like siliciclastics and radiolarites. Downsection, in the Oligocene between 30 and 25 Ma, the strong contribution from dolomites extended further to the west (Section 3). In Section 5, the contribution from dolomites to the total sedimentary fragments is low (see also MgO/SiO_2 ratios, Fig. 8) implying that the extent of typical Austroalpine sedimentary cover nappes (Northern Calcareous Alps, Fig. 1) to the west was already limited in Oligocene times. Instead, chert grains are quite frequent at 27–26 Ma in Section 5, probably reflecting the contribution from siliceous limestones. Such lithologies were reported from conglomerates of similar age (Schlunegger *et al.*, 1998).

A distinct break in time in the eastern sections can be observed at ≈21 Ma (Fig. 14). Although detritus from sedimentary sources still remains predominant, a significant contribution from ultramafic and (meta)basaltic rocks of MOR to intraplate affinity is documented by light mineral composition and chemical data. (Ultra)mafic lithologies are typical of Penninic ophiolitic complexes (e.g. Arosa zone, Fig. 1). This change coincides with a considerable increase in epidote and with the first contribution of 'greenstone' conglomerate clasts (see above; Kempf *et al.*, 1999). The compositional change at ≈21 Ma suggests that the rivers draining the eastern source region cut into Penninic ophiolitic rocks by this time, but Austroalpine dolomite rocks were still exposed in large parts of the hinterland. The small peak of granitoid-derived material

between ≈22 and ≈18 Ma most probably reflects erosion of slivers of Austroalpine crystalline rocks shortly before the downcutting reached Penninic rocks.

Two further distinct breaks occurred in the central part of the basin and in the corresponding hinterland at ≈25 Ma and ≈20 Ma (Fig. 14). At ≈25 Ma, the dominant contribution from sedimentary source rocks changed to dominantly feldspar-rich granitoids, occurring abruptly in Section 3 and more gradually in Section 5. The origin of granitoid, gneissic and quartzite pebbles in the post-25 Ma sediments of Section 5 is still a matter of debate. Schlunegger *et al.* (1998) located the source of at least the quartzites in the Penninic Grand St Bernard nappe in the hangingwall of the Simplon Fault (Fig. 1), whereas Spiegel *et al.* (2001) suggested a Lower Austroalpine source for the granitoid rocks, based on zircon fission track cooling data. von Eynatten & Wijbrans (2003) argued in favour of a Penninic origin of granitoids in Section 5, because detrital white micas from this and more westerly sections show frequent Lower Permian $^{40}Ar/^{39}Ar$ cooling ages, which are more typical of Penninic crystalline sources. However, the question remains open, and a possible erosion of contrasting crystalline basement lithologies may also be considered. Despite this controversy, it is clear that rivers draining the central part had already cut into the crystalline basement at ≈25 Ma, and that the removal of the sedimentary cover at the time of downcutting into the basement was more complete in the central than in the eastern hinterland.

At ≈20 Ma, the erosion of granitoid rocks in the central hinterland decreased significantly, as shown by the sediment composition in Sections 4 and 6. In Section 4, this decrease was accompanied by an increased contribution from low-grade metasedimentary rocks. In Section 6, the decrease in granitoid fragments was accompanied by an increase in more local debris. The latter marks the initiation of the Guggershörnli fan at ≈19 Ma in front of thrusted Subalpine Molasse sheets (Strunck, 2001). The marked change in sediment composition at ≈20 Ma is accompanied by the first occurrence of white mica with Tertiary $^{40}Ar/^{39}Ar$ cooling ages, pointing to the exhumation of the Lepontine metamorphic dome (von Eynatten & Wijbrans, 2003; see next section).

In the westernmost Section 7, granitoid-derived detritus was already common at ≈28 Ma together with detritus from Penninic (ultra)mafic source rocks, partly affected by high-pressure metamorphism (Fig. 14). These sediments were delivered by the axial Lake Geneva drainage system. As discussed earlier, the entry point of material into the SMB is thought to be located somewhere to the SW of Lake Geneva. Chrome spinel chemistry suggests that the ultramafic to mafic source rocks had a MOR affinity (Fig. 13). Such rocks are widespread in the (South Penninic) Piemonte zone of the western Alps (Combin zone, Zermatt-Saas zone and southern equivalents, e.g. Pfeifer *et al.*, 1989) and are structurally located directly below the Austroalpine Dent-Blanche nappe (Dal Piaz *et al.*, 2001; Fig. 1). Zircon FT ages from the present-day exposed Dent-Blanche nappe are generally >30 Ma (Hurford *et al.*, 1991) and indicate a phase of rapid cooling after peak metamorphism, which is dated at 40–36 Ma (Markley *et al.*, 1998; Desmons *et al.*, 1999). Because the Austroalpine–Penninic nappe stack probably extended further to the west in Oligocene times (Mange-Rajetzky & Oberhänsli, 1982), erosion of Piemonte zone ophiolites is considered as the most likely source for (ultra)mafic detritus in ≈28 Ma sediments of the westernmost Section 7.

Exhumation of the Lepontine dome

The exhumation of the Lepontine metamorphic dome is considered to have caused a major structural and morphological reorganization of the Miocene Central Alps (Schlunegger *et al.*, 1998; Kuhlemann *et al.*, 2001). Enhanced cooling and exhumation occurred between 18 and 15 Ma (Grasemann & Mancktelow, 1993). Cooling rates increased continuously up to ≈40 °C/Ma between ≈19 and ≈14 Ma based on geochronological data of detrital minerals from the central SMB (Fig. 15; von Eynatten & Wijbrans, 2003). These detrital minerals were delivered from low-grade metamorphic rocks of the Miocene Lepontine area into the SMB and, consequently, the Miocene drainage divide was located south of the northern margin of the Lepontine.

The beginning of the Lepontine exhumation is reflected in the sandstone composition by an increase in low-grade metasedimentary lithoclasts (L_{sm}) in sediments younger than ≈20 Ma from the central SMB (Figs 5 and 14). These clasts are interpreted as being derived from the former upper levels of the present-day Lepontine (von Eynatten *et al.*, 1999). The widespread exposure of crystalline rocks, accompanied by the almost complete removal of the sedimentary cover in the central hinterland at ≈25 Ma, may be interpreted as the first signal of the doming of the Lepontine area.

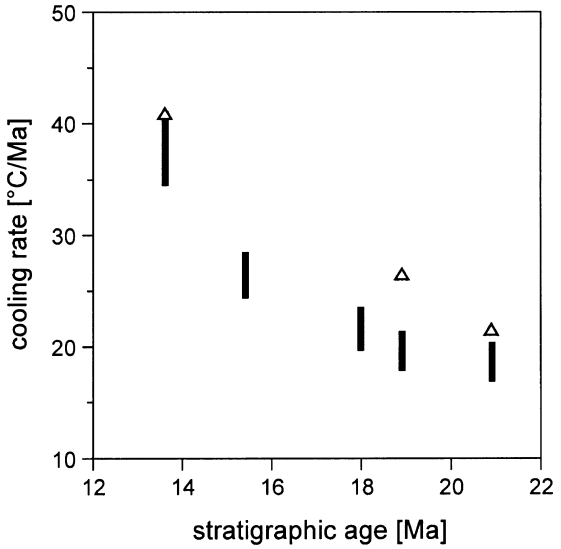

Fig. 15. Plot of cooling rates vs. stratigraphic ages obtained for detrital minerals in sediments from central Section 4 (modified after von Eynatten & Wijbrans, 2003). Cooling rates are calculated based on $^{40}Ar/^{39}Ar$ white mica ages (black bars, $T_c = 350–420$ °C) and zircon fission track model ages (triangles, $T_c = 240$ °C; Spiegel *et al.*, 2000).

CONCLUSIONS

A multidisciplinary approach, using light and heavy mineral analysis, whole-rock and mineral geochemistry identifies a diversity of source rocks for the proximal sandstones of the Swiss Molasse Basin (SMB) including:

1 carbonates (mostly Austroalpine dolomites), recorded by carbonate lithoclasts and high MgO/SiO_2 ratios in the sandstones;

2 flysch-like siliciclastics signalled by sedimentary siliciclastic lithoclasts, the occurrence of recycled chrome spinel, high Cr/Ni ratios and high ZTR values;

3 Penninic (ultra)mafic rocks indicated by serpentinite and mafic volcanic clasts, high Cr/Ba and/or Ni/Ba ratios and first-cycle chrome spinel of MOR or intraplate origin;

4 feldspar-rich granitoids, recorded by frequent feldspar grains, felsic plutonic clasts and high Na_2O/SiO_2 ratios; and

5 low-grade metasedimentary rocks indicated by foliated quartz–chlorite–mica aggregates.

Variations in these source rocks in space and time place constraints on the Oligocene to Miocene evolution of the Central Alps. Sandstones from the eastern part of the SMB document a normal unroofing sequence (*sensu* Colombo, 1994) with downcutting from Austroalpine sedimentary cover into Austroalpine crystalline rocks and, slightly later at ≈21 Ma, also into Penninic ophiolites. In the central part, downcutting into crystalline basement rocks occurred at ≈25 Ma, and the removal of the sedimentary cover was much more advanced compared with that in the east. This may be interpreted as the first signal from the updoming of the Lepontine area. The nature of the sedimentary cover was also different given the very low contribution of Austroalpine dolomite rocks compared with the east. At ≈20 Ma, extensional tectonics in the hinterland of the central part of the SMB led to the first exposure of low-grade metamorphic rocks from the footwall of the Simplon Fault in the Central Alps. Erosion of these rocks persisted up to the deposition of the youngest sediments at ≈13 Ma. Further to the west, contribution from granitoid and (ultra)mafic rocks is documented as early as ≈28 Ma. The source for the (ultra)mafic detritus in the western part was the Penninic ophiolites of the Piemonte zone of the western Alps, which were already exposed to the surface at ≈28 Ma.

Whole-rock chemical and light mineral data used in this study permitted the reconstruction of major source rocks and their variation in space and time, whereas heavy mineral analysis proved less precise in source rock discrimination because some of the heavy mineral species (e.g. chrome spinel, epidote, garnet) occur in more than one source lithology. Mineral chemistry provides valuable additional information on source rock petrology.

ACKNOWLEDGEMENTS

This study was supported by the Deutsche Forschungsgemeinschaft (grant EY 23/1). Field work strongly benefited from guidance and advice from Oliver Kempf, Fritz Schlunegger and Peter Strunck. Sigrid Bergmann and Frank Linde are thanked for continuous technical support. I greatly appreciate comments and the stimulation provided by Giorgio V. Dal Piaz, Reinhard Gaupp, Oliver Kempf, Conny Spiegel and Thomas Voigt. A thorough presubmission review by Fritz Schlunegger as well as substantial reviews by Gary H. Girty and Maria Mange helped to improve an earlier version of the paper.

SUPPLEMENTARY MATERIAL

The following material is available from http://www.blackwellpublishing.com/products/journals/suppmat/sed/sed571/sed571sm.htm

Table S1. Sandstone framework (light mineral data).

Table S2. Heavy mineral data.

Table S3. Major and trace element XRF data.

REFERENCES

Allen, P.A., Mange-Rajetzky, M., Matter, A. and **Homewood, P.** (1985) Dynamic paleogeography of the open Burdigalian seaway, Swiss Molasse basin. *Eclogae Geol. Helv.*, **78,** 351–381.

Arai, S. (1992) Chemistry of chromian spinel in volcanic rocks as a potential guide to magma chemistry. *Min. Mag.*, **56,** 173–184.

Baudin, T., Marquer, D. and **Persoz, F.** (1993) Basement-cover relationships in the Tambo nappe (Central Alps, Switzerland): geometry, structure, and kinematics. *J. Struct. Geol.*, **15,** 543–553.

Berger, J.-P. (1996) Cartes paléogeographiques-palinspastiques du bassin molassique suisse (Oligocène inférieur–Miocéne moyen). *Neues Jb. Geol. Paläont. Abh.*, **202,** 1–44.

Berggren, W.A., Kent, D.V., Swisher, C.C. and **Aubry, M.-P.** (1995) A revised Cenozoic geochronology and chronostratigraphy. In: *Geochronology, Time Scales, and Global Stratigraphic Correlations* (Eds W.A. Berggren, D.V. Kent, M.-P. Aubry and J. Hardenbohl), *SEPM Spec. Publ.*, **54,** 17–28.

Burbank, D.W., Engesser, A., Matter, A. and **Weidmann, M.** (1992) Magnetostratigraphic chronology, mammalian faunas, and stratigraphic evolution of the Lower Freshwater Molasse, Haute Savoie, France. *Eclogae Geol. Helv.*, **85,** 399–431.

Burkhard, M. and **Sommaruga, A.** (1998) Evolution of the western Swiss Molasse basin: structural relations with the Alps and the Jura belt. In: *Cenozoic Foreland Basins in Western Europe* (Ed. A. Mascle, C. Puigdefábregas, H.P. Luterbacher and M. Fernàndez), *Geol. Soc. London Spec. Publ.*, **134,** 279–298.

Colombo, F. (1994) Normal and reverse unroofing sequences in syntectonic conglomerates as evidence of progressive basinward deformation. *Geology*, **22,** 235–238.

Dal Piaz, G.V. (1999) The Austroalpine-Piedmont nappe stack and the puzzle of Alpine Tethys. *Mem. Sci. Geol.*, **51,** 155–176.

Dal Piaz, G.V., Cortiana, G., Del Moro, A., Martin, S., Pennacchioni, G. and **Tartarotti, P.** (2001) Tertiary age and paleostructural inferences of the eclogitic imprint in the Austroalpine outliers and Zermatt-Saas ophiolite, western Alps. *Int. J. Earth Sci.*, **90,** 668–684.

Decker, J. and **Helmold, K.P.** (1985) The effect of grain size on detrital modes: a test of the Gazzi-Dickinson point-counting method – discussion. *J. Sed. Petrol.*, **55,** 618–620.

Desmons, J., Aprahamian, J., Compagnoni, R., Cortesogno, L. Frey, M. (1999) Alpine metamorphism of the Western Alps. I. Middle to high T/P metamorphism. *Schweiz. Mineral. Petrogr. Mitt.*, **79,** 89–110.

von Eynatten, H. (1996) *Provenanzanalyse kretazischer Siliziklastika aus den Nördlichen Kalkalpen: Petrographie, Mineralchemie und Geochronologie des frühalpidisch umgelagerten Detritus*. PhD Thesis, University of Mainz, Mainz, 145 pp.

von Eynatten, H. and **Gaupp, R.** (1999) Provenance of Cretaceous synorogenic sandstones in the Eastern Alps: constraints from framework petrography, heavy mineral analysis, and mineral chemistry. *Sed. Geol.*, **124,** 81–111.

>von Eynatten, H. and **Wijbrans, J.R.** (2003) Precise tracing of exhumation and provenance using Ar/Ar-geochronology of detrital white mica: the example of the Central Alps. In: *Tracing Tectonic Processes Using the Sedimentary Record* (Eds T. McCann and A. Saintot), *Geol. Soc. London Spec. Publ.*, **208,** 289–305.

von Eynatten, H., Schlunegger, F., Gaupp, R. and **Wijbrans, J.R.** (1999) Exhumation of the Central Alps: evidence from $^{40}Ar/^{39}Ar$ laserprobe dating of detrital white micas from the Swiss Molasse Basin. *Terra Nova*, **11,** 284–289.

Frey, M. and **Ferreiro Mählmann, R.** (1999) Alpine metamorphism of the Central Alps. *Schweiz. Mineral. Petrogr. Mitt.*, **79,** 135–154.

Frisch, W., Ring, U., Dürr, S., Borchert, S. and **Biehler, D.** (1994) The Arosa zone and Platta nappe ophiolites (Eastern Swiss Alps). Geochemical characteristics and their meaning for the evolution of the Penninic ocean. *J. Geol. Bundesanstalt Wien*, **137,** 19–33.

Füchtbauer, H. (1964) Sedimentpetrographische Untersuchungen in der älteren Molasse nördlich der Alpen. *Eclogae Geol. Helv.*, **57,** 157–298.

Füchtbauer, H. (1967) Die Sandsteine in der Molasse nördlich der Alpen. *Geol. Rundsch.*, **56,** 266–300.

Garver, J.I., Royce, P.R. and **Smick, T.A.** (1996) Chromium and nickel in shale of the Taconic foreland: a case study for the provenance of fine-grained sediments with an ultramafic source. *J. Sed. Res.*, **66,** 100–106.

Gasser, U. (1967) Erste Resultate über die Verteilung von Schwermineralen in verschiedenen Flyschkomplexen der Schweiz. *Geol. Rundsch.*, **56,** 300–308.

Gasser, U. (1968) Die innere Zone der Subalpinen Molasse des Entlebuchs (Kt. Luzern), Geologie und Sedimentologie. *Eclogae Geol. Helv.*, **61,** 229–313.

Gaupp, R. (1980) *Sedimentpetrographische und stratigraphische Untersuchungen in den oberostalpinen Mittelkreide-Serien des Westteils der Nördlichen Kalkalpen*. PhD Thesis. Technical University of Munich, Munich, 282 pp.

Gebauer, D. (1999) Alpine geochronology of the Central and Western Alps: new constraints for a complex geodynamic evolution. *Schweiz. Mineral. Petrogr. Mitt.*, **79,** 191–208.

Grantham, J.H. and **Velbel, M.A.** (1988) The influence of climate and topography on rock-fragment abundance in modern fluvial sands of the southern Blue Ridge Mountains, North Carolina. *J. Sed. Petrol.*, **58,** 219–227.

Grasemann, B. and **Mancktelow, N.S.** (1993) Two-dimensional thermal modelling of normal faulting: the Simplon Fault Zone, Central Alps, Switzerland. *Tectonophysics*, **225,** 155–165.

Homewood, P., Allen, P.A. and **Williams, G.D.** (1986) Dynamics of the Molasse basin of western Switzerland. In: *Foreland Basins* (Eds P.A. Allen and P. Homewood), *Int. Assoc. Sedimentol. Spec. Publ.*, **8,** 199–217.

Hurford, A.J., Flisch, M. and **Jäger, E.** (1989) Unravelling the thermo-tectonic evolution of the Alps: a contribution from fission track analysis and mica dating. In: *Alpine Tectonics*

(Eds M. Coward, D. Dietrich and R.G. Park), *Geol. Soc. London Spec. Publ.*, **45,** 369–398.

Hurford, A.J., Hunziker, J.C. and **Stöckhert, B.** (1991) Constraints on the late thermotectonic evolution of the Western Alps: evidence for episodic uplift. *Tectonics*, **10,** 758–769.

Hyndman, D.W. (1985) *Petrology of Igneous and Metamorphic Rocks*, 2nd edn. McGraw-Hill, New York.

Ingersoll, R.V., Bullard, T.F., Ford, R.L., Grimm, J.P., Pickle, J.D. and **Sares, S.W.** (1984) The effect of grain size on detrital modes: a test of the Gazzi-Dickinson point-counting method. *J. Sed. Petrol.*, **54,** 103–116.

Johnsson, M.J. (1993) The system controlling the composition of clastic sediments. In: *Processes Controlling the Composition of Clastic Sediments* (Eds M.J. Johnsson and A. Basu), *Geol. Soc. Am. Spec. Paper*, **284,** 1–19.

Johnsson, M.J., Stallard, R.F. and **Lundberg, N.** (1991) Controls on the composition of fluvial sands from a tropical weathering environment: Sands from the Orinoco river drainage basin, Venezuela and Columbia. *Geol. Soc. Am. Bull.*, **103,** 1622–1647.

Kempf, O. (1998) *Magnetostratigraphy and facies evolution of the Lower Freshwater Molasse (USM) of eastern Switzerland*. PhD Thesis, University of Berne, Berne, 138 pp.

Kempf, O., Bolliger, T., Kälin, D., Engesser, B. and **Matter, A.** (1997) New magnetostratigraphic calibration of Early to Middle Miocene mammal biozones of the North Alpine foreland basin. In: *Actes du Congrès Biochrom'97* (Eds J.-P. Aguilar, S. Legendre and J. Michaux), *Mém. Trav. EPHE Inst. Montpellier*, **21,** 547–561.

Kempf, O., Matter, A., Burbank, D.W. and **Mange, M.** (1999) Depositional and structural evolution of a foreland basin margin in a magnetostratigraphic framework: the eastern Swiss Molasse Basin. *Int. J. Earth Sci.*, **88,** 253–275.

Kuhlemann, J., Frisch, W., Dunkl, I. and **Székely, B.** (2001) Quantifying tectonic versus erosive denudation by the sediment budget: the Miocene core complexes of the Alps. *Tectonophysics*, **330,** 1–23.

Kuhlemann, J. and **Kempf, O.** (2002) Post-Eocene evolution of the North Alpine foreland basin and its response to Alpine tectonics. *Sed. Geol.*, **152,** 45–78.

McBride, E.F. (1963) A classification of common sandstones. *J. Sed. Petrol.*, **33,** 664–669.

Mange, M.A. and **Maurer, H.F.W.** (1991) *Schwerminerale in Farbe*. Enke, Stuttgart.

Mange-Rajetzky, M. and **Oberhänsli, R.** (1982) Detrital lawsonite and blue sodic amphibole in the Molasse of Savoy, France, and their significance in assessing Alpine evolution. *Schweiz. Mineral. Petrogr. Mitt.*, **62,** 415–436.

Markley, M.J., Teyssier, C., Cosca, M.A., Caby, R., Hunziker, J.C. and **Sartori, M.** (1998) Alpine deformation and $^{40}Ar/^{39}Ar$ geochronology of synkinematic white mica in the Siviez-Mischabel nappe, western Pennine Alps, Switzerland. *Tectonics*, **17,** 407–425.

Matter, A. (1964) Sedimentologische Untersuchungen im östlichen Napfgebiet. *Eclogae Geol. Helv.*, **57,** 315–428.

Maurer, H. (1983) Sedimentpetrographische Analysen an Molasseabfolgen der Westschweiz. *Jb. Geol. Bundesanstalt Wien*, **126,** 23–69.

Michalski, I. and **Soom, M.** (1990) The Alpine thermo-tectonic evolution of the Aar and Gotthard massifs, Central Switzerland. Fission track ages on zircon and apatite and K-Ar mica ages. *Schweiz. Mineral. Petrogr. Mitt.*, **70,** 373–387.

von Moos, A. (1935) Sedimentpetrographische Untersuchungen an Molassesandsteinen. *Schweiz. Mineral. Petrogr. Mitt.*, **15,** 169–265.

Morton, A.C. and **Hallsworth, C.** (1994) Identifying provenance-specific features of detrital heavy mineral assemblages in sandstones. *Sed. Geol.*, **90,** 241–256.

Najman, Y. and **Garzanti, E.** (2000) Reconstructing early Himalayan tectonic evolution and paleogeography from Tertiary foreland basin sedimentary rocks, northern India. *Geol. Soc. Am. Bull.*, **112,** 435–449.

Pfeifer, H.R., Colombi, A. and **Ganguin, J.** (1989) Zermatt-Saas and Antrona zone. A petrographic and geochemical comparison of polyphase metamorphic ophiolites of the West-Central Alps. *Schweiz. Mineral. Petrogr. Mitt.*, **69,** 217–236.

Pfiffner, O.A. (1986) Evolution of the north Alpine foreland basin in the Central Alps. In: *Foreland Basins* (Eds P.A. Allen and P. Homewood), *Int.* Assoc. *Sedimentol. Spec. Publ.*, **8,** 219–228.

Rollinson, H. (1993) *Using Geochemical Data*. Longman, Essex.

Schlunegger, F. (1995) *Magnetostratigraphische und fazielle Entwicklung der Unteren Süßwassermolasse zwischen Aare und Limmat*. PhD Thesis, University of Berne, Berne, 185 pp.

Schlunegger, F. (1999) Controls of surface erosion on the evolution of the Alps: constraints from the stratigraphies of the adjacent foreland basins. *Int. J. Earth Sci.*, **88,** 285–304.

Schlunegger, F., Matter, A. and **Mange, M.A.** (1993) Alluvial fan sedimentation and structure of the southern Molasse basin margin, Lake Thun area, Switzerland. *Eclogae Geol. Helv.*, **86,** 717–750.

Schlunegger, F., Burbank, D.W., Matter, A., Engesser, B. and **Mödden, C.** (1996) Magnetostratigraphic calibration of the Oligocene to Middle Miocene (30–15 Ma) mammal biozones and depositional sequences of the Swiss Molasse Basin. *Eclogae Geol. Helv.*, **89,** 753–788.

Schlunegger, F., Matter, A., Burbank, D.W. and **Klaper, E.M.** (1997) Magnetostratigraphic constraints on relationships between evolution of the central Swiss Molasse basin and Alpine orogenic events. *Geol. Soc. Am. Bull.*, **109,** 225–241.

Schlunegger, F., Slingerland, R. and **Matter, A.** (1998) Crustal thickening and crustal extension as controls on the evolution of the drainage network of the central Swiss Alps between 30 Ma and the present: constraints from the stratigraphy of the North Alpine Foreland Basin and the structural evolution of the Alps. *Basin Res.*, **10,** 197–212.

Schmid, S.M., Pfiffner, O.A., Froitzheim, N., Schönborn, G. and **Kissling, E.** (1996) Geophysical-geological transect and tectonic evolution of the Swiss-Italian Alps. *Tectonics*, **15,** 1036–1064.

Sinclair, H.D. and **Allen, P.A.** (1992) Vertical versus horizontal motions in the Alpine orogenic wedge: stratigraphic response in the foreland basin. *Basin Res.*, **4,** 215–232.

Spiegel, C., Kuhlemann, J., Dunkl, I., Frisch, W., von Eynatten, H. and **Balogh, K.** (2000) Erosion history of the Central Alps: evidence from zircon fission track data of the foreland basin sediments. *Terra Nova*, **12,** 163–170.

Spiegel, C., Kuhlemann, J., Dunkl, I. and **Frisch, W.** (2001) Paleogeography and catchment evolution in a mobile orogenic belt: the Central Alps in Oligo-Miocene times. *Tectonophysics*, **341,** 33–47.

Spiegel, C., Siebel, W., Frisch, W. and **Zsolt, B.** (2002) Nd and Sr isotopic ratios and trace element geochemistry of epidote from the Swiss Molasse Basin as provenance indicators: implications for the reconstruction of the exhumation history of the Central Alps. *Chem. Geol.*, **189,** 231–250.

Steck, A. and **Hunziker, J.** (1994) The Tertiary structural and thermal evolution of the Central Alps – compressional and

extensional structures in an orogenic belt. *Tectonophysics*, **238,** 229–254.

Strunck, P. (2001) *The Molasse of western Switzerland*. PhD Thesis. University of Berne, Berne, 246 pp.

Weltje, G.J., Meijer, X.D. and **de Boer, P.L.** (1998) Stratigraphic inversion of siliciclastic basin fills: a note on the distinction between supply signals resulting from tectonic and climatic forcing. *Basin Res.*, **10,** 129–153.

Zuffa, G.G. (1980) Hybrid arenites: their composition and classification. *J. Sed. Petrol.*, **50,** 21–29.

Manuscript received 16 April 2002;
revision accepted 23 January 2003.